Available online at www.sciencedirect.com
ScienceDirect
Comput. Methods Appl. Mech. Engrg. 407 (2023) 115932
Computer methods in applied mechanics and engineering
www.elsevier.com/locate/cma

An isogeometric boundary element formulation for stress concentration problems in couple stress elasticity

G. Hattori[a], J. Trevelyan[a,*], P.A. Gourgiotis[b]

[a] *Department of Engineering, Durham University, Durham DH1 3LE, UK*
[b] *Department of Civil Engineering, University of Thessaly, Pedion Areos, GR 38334, Volos, Greece*

Received 6 December 2022; received in revised form 28 January 2023; accepted 30 January 2023
Available online xxxx

Abstract

An isogeometric boundary element method (IGABEM) is developed for the analysis of two-dimensional linear and isotropic elastic bodies governed by the couple stress theory. This theory is the simplest generalized continuum theory that can effectively model size effects in solids. The couple stress fundamental solutions are explicitly derived and used to construct the boundary integral equations. A new boundary integral equation arises to obtain the moments and rotations introduced by the couple stress formulation. A new analytical solution is also derived in the present work for an elliptical opening in an infinite sheet under uniaxial far-field stress. Several stress concentration problems are examined to illustrate and validate the application of the IGABEM in couple stress elasticity. It is shown that the IGABEM scheme exhibits advantageous convergence properties in comparison with the conventional BEM for boundary value problems within the framework of couple stress elasticity.

Keywords: Couple stress; Boundary element method; Isogeometric

1. Introduction

In the present work, an isogeometric boundary element method (IGABEM) is developed for the first time for plane-strain problems in the context of linear and isotropic couple stress elasticity. The couple stress theory of elasticity, also known as Cosserat theory with constrained rotations, is the simplest gradient theory in which couple stresses make their appearance. The theory was developed in rudimentary form by the Cosserat brothers [1] but the subject reached maturity with the seminal works of Toupin [2] and Mindlin [3]. The couple stress theory assumes an augmented form of the Euler–Cauchy principle with a non-vanishing couple traction, and a strain–energy density that depends upon both the strain and the gradient of rotation. Such assumptions are appropriate for materials with granular and layered structures, where the interaction between adjacent elements may introduce internal moments. It is noted that the couple stress theory is different from the micropolar (or Cosserat) theory that takes material particles with six independent degrees of freedom (three displacement components and three rotation components, the latter involving rotation of a micro-medium with respect to its surrounding medium). Due to the presence of couple stresses, characteristic material lengths appear in the constitutive equations of the theory that

* Corresponding author.
E-mail address: jon.trevelyan@durham.ac.uk (J. Trevelyan).

https://doi.org/10.1016/j.cma.2023.115932

can be related to the material microstructure. The presence of these characteristic lengths implies that the couple stress theory encompasses the analytical possibility of size effects which are absent in the classical theory. Recent studies provide an account of the determination of the characteristic lengths of couple stress theory and related gradient theories via homogenization of heterogeneous materials (see e.g. [4–7]). The couple stress theory has been successfully employed recently to model microstructured materials and pertinent size effects in various areas such as fracture [8–11], contact [12–17], stress/strain localization [18–21], and wave propagation problems [22,23].

The Boundary Element Method (BEM) is a powerful and efficient method for solving many engineering problems, offering an efficient alternative to the FEM. In the last decades, the boundary element method has been successfully employed for the solution of a multitude of boundary value problems in the frame of different generalized continuum theories. Most of the works are within the context of micropolar theory (see, for example, [24–28]), with a few works within strain-gradient elasticity [29–31]. However, to the authors' best knowledge, no works exist using the boundary element method in the context of the standard couple stress theory. Mention here should be made to the works by Hadjesfandiari and Dargush [32], and Lei et al. [33,34] who treat plane strain problems using a boundary element approach within the frame of a variant model of the standard couple stress theory proposed by Hadjesfandiari and Dargush [35]. In this model the couple stress tensor is considered to be skew-symmetric supposedly eliminating the "inconsistency" of the couple stress theory regarding the indeterminacy of the isotropic part of the couple stress tensor and accordingly the antisymmetric part of the stress tensor. However, as Neff et al. [36] point out, the authors use an incomplete set of boundary conditions in their virtual work approach. In particular, they assume that the normal component of the couple stress tensor m_{nn} is zero on the boundary, a claim which is not supported by any variational argument. This leads to different field equations and a different set of boundary conditions than those rigorously derived by Toupin [2], Mindlin [3], and Koiter [37]. Note that as Muki and Sternberg [38] showed (see Eqs. (2.13)-(2.15) in their paper), the couple stress tensor is unique, apart from an arbitrary additive *constant* isotropic couple stress field, and hence the antisymmetric part of the stress becomes fully determinate, showing therefore that no inconsistency occurs in the standard couple stress theory. The latter conclusion is also reached by Neff et al. [36] (Section 8, in their work). Moreover, as Mindlin [39] points out the standard couple stress theory can be formally derived from the Form III type of gradient elasticity by setting to zero the supersymmetric part of the second gradient of the displacement ($\bar{\kappa}_{ijk} = 0$). Finally, we remark that in the particular case of plane strain, where only the deviatoric part of the couple stress tensor enters the governing equations, the model of Hadjesfandiari and Dargush [35] happens to yield the same field equations and boundary conditions in terms of the displacements as in the standard couple stress theory. Nonetheless, in the case of antiplane strain or in the general 3D case, the equations are different and the results obtained using the model presented in [35] should be treated with caution.

As was shown by Simpson et al. [40], the advantages of isogeometric methods found in the FEM extend readily to elastic analysis with the BEM. The resulting analysis method is called IGABEM (isogeometric analysis boundary element method) where non-uniform rational B-splines (NURBS) are employed as shape functions for geometry parameterization and approximation of the field variables. The IGABEM has great potential for the simulation of elasticity problems because of its exact geometric representation and good approximation properties. Moreover, the IGABEM is well suited for tackling problems within the framework of generalized continuum theories due to the high-order continuity requirements of the field equations that occur in such theories. Indeed, as we shall see in Section 2, the couple stress theory is governed by a fourth order differential operator as compared to the classical Navier–Cauchy operator which is of the second order.

The paper is organized as follows. In Section 2 the governing equations of the standard couple stress elasticity theory under plane strain conditions are presented. Then in Section 3, the fundamental plane strain solutions (Green's functions) for a concentrated force and a concentrated moment are derived in closed form using a Fourier transform analysis (see also Appendix A). In Section 4, the two boundary integral equations for the displacement vector and the rotation are obtained and closed form expressions are provided for the free terms (see also Appendix B). In Section 5, an IGABEM discretization is developed for plane strain isotropic couple stress materials. In Section 6, an analytical solution of the plane strain problem of an elliptical hole in an infinite couple stress material is derived using series of Mathieu functions and the Schmidt orthogonalization process. Finally, in Section 7 various stress concentration problems are examined involving couple stress materials with circular and elliptical holes. It is shown that the IGABEM scheme exhibits advantageous convergence properties in comparison with the conventional polynomial BEM formulation developed also in this study for comparison purposes. A comparison of the present results with the classical elasticity solutions is also provided illustrating the well observed stiffening size-effects in problems when the geometrical defects become comparable to the characteristic material length of the theory.

2. Plane-strain couple stress elasticity

In this Section we recall briefly the main elements of the plane strain isotropic couple stress elasticity. More detailed expositions of the theory can be found in the works of Toupin [2], Mindlin and Tiersten [3], and Koiter [37] (see also [10,22]).

For a body that occupies a closed domain Ω in the (x_1, x_2)-plane with a boundary Γ, and under conditions of plane strain, the displacement field takes the general form

$$u_q \equiv u_q(x_1, x_2) \neq 0, \quad u_3 \equiv 0. \tag{1}$$

Note that henceforth all Latin indices span the range (1,2), subscripts preceded by a comma denote differentiation with respect to pertinent Cartesian variable, and the summation convention is assumed throughout unless otherwise noted. Accordingly, the governing kinematic relations in the framework of the geometrically linear theory become

$$\varepsilon_{pq} = \frac{1}{2}(u_{q,p} + u_{p,q}), \quad \varepsilon_{p3} = 0, \quad \varepsilon_{33} = 0 \tag{2}$$

$$\omega = \frac{1}{2} e_{pq} u_{q,p}, \quad \kappa_q = \omega_{,q} \tag{3}$$

where ε_{pq} are the components of the usual strain tensor, $\omega \equiv \omega_3$ is the rotation, and $\kappa_q \equiv \kappa_{q3}$ are the non-vanishing components of the curvature tensor (i.e. the gradient of rotation). Also, e_{pq} is the 2D permutation tensor ($e_{11} = e_{22} = 0$, $e_{12} = -e_{21} = 1$).

Further, the stress equations of equilibrium reduce to

$$\sigma_{pq,p} + X_q = 0, \quad e_{pq}\sigma_{pq} + m_{p,p} + Y = 0, \tag{4}$$

where σ_{pq} and $m_p \equiv m_{p3}$ are the components of the (asymmetric) stress and couple stress tensors, respectively, in the case of plane strain. Moreover, X_q is the in-plane body force and $Y \equiv Y_3$ is the out-of-plane component of the body couple.

For a homogeneous, centrosymmetric and isotropic linear couple stress material the constitutive equations furnish

$$\sigma_{(pq)} = \frac{2\mu\nu}{1-2\nu}\delta_{pq}\varepsilon_{kk} + 2\mu\varepsilon_{pq}, \quad \sigma_{33} = \nu\sigma_{kk}, \tag{5}$$

and

$$m_q = 4\mu\ell^2\kappa_q, \tag{6}$$

where δ_{pq} is the Kronecker delta, $\sigma_{(pq)}$ is the symmetric part of the stress tensor, μ is the shear modulus, ν is the Poisson's ratio, and ℓ is the characteristic material length of couple stress theory. The antisymmetric part $\sigma_{[pq]}$ of the stress tensor can be readily found from Eq. $(4)_2$ and is given, in conjunction with (3) as

$$\sigma_{[pq]} = -\frac{1}{2}e_{pq}m_{k,k} - \frac{1}{2}e_{pq}Y = -2\mu\ell^2 e_{pq}\nabla^2\omega - \frac{1}{2}e_{pq}Y. \tag{7}$$

The total stress is written as $\sigma_{pq} = \sigma_{(pq)} + \sigma_{[pq]}$. Regarding the traction boundary conditions at any point on a smooth boundary or section, the following two in-plane force-tractions t_q and one out-of-plane couple-traction $\mathfrak{s} \equiv \mathfrak{s}_3$ should be specified

$$t_q = \sigma_{pq}n_p, \quad \mathfrak{s} = m_q n_q, \tag{8}$$

where n_q are the components of the outward unit normal to the boundary.

Finally, combining Eqs (2)–(7), we derive the following system of coupled fourth order PDEs for the displacement field [41]

$$\mu\left(\nabla^2 u_q + (1-2\nu)^{-1}u_{p,pq} + \ell^2 e_{qp}e_{mn}\nabla^2 u_{n,pm}\right) + X_q + \frac{1}{2}e_{qp}Y_{,p} = 0, \tag{9}$$

where ∇^2 is the two-dimensional Laplace operator.

3. Fundamental solutions

The field equations governing plane-strain deformations in the case of a couple stress material admit two infinite-body Green's functions: one for an in-plane concentrated unit force ($\mathcal{F}$) and one for an out-of-plane concentrated unit couple ($\mathcal{M}$). A closed form solution in both cases is obtained by employing the double exponential Fourier transform. The detailed derivation of the Green's functions is given in Appendix A.

3.1. Concentrated force

Consider now $u_q = U_{qk}^{(\mathcal{F})}(\boldsymbol{x},\boldsymbol{\xi})\boldsymbol{e}_k$ the component of displacement in the qth direction at the point $\boldsymbol{x}$ caused by a unit force ($\mathcal{F}$) acting in the kth direction at point $\boldsymbol{\xi}$. The displacement field in this case assumes the following form

$$\begin{aligned} U_{qk}^{(\mathcal{F})} =& \frac{1}{8\pi\mu(1-\nu)}\left[r_{,q}r_{,k} - (3-4\nu)\delta_{qk}\ln r\right] \\ &- \frac{1}{2\pi\mu}\left[\left(r_{,q}r_{,k} - \frac{1}{2}\delta_{qk}\right)\left(\frac{2\ell^2}{r^2} - K_2\left[\frac{r}{\ell}\right]\right) + \frac{1}{2}\delta_{qk}K_0\left[\frac{r}{\ell}\right]\right], \end{aligned} \tag{10}$$

where $\boldsymbol{r} = \boldsymbol{x} - \boldsymbol{\xi}$, with Cartesian components $r_q = x_q - \xi_q$ and magnitude $r = (r_q r_q)^{1/2}$, so that $r_{,q} = \partial r/\partial x_q = r_q r^{-1}$, and $K_n[\cdot]$ is the modified second kind Bessel function of the nth-order.

Accordingly, the strain tensor and the rotation vector become

$$\begin{aligned} E_{pqk}^{(\mathcal{F})} =& -\frac{1}{8\pi\mu(1-\nu)r}\left[(1-2\nu)(r_{,q}\delta_{pk} + r_{,p}\delta_{qk}) - r_{,k}\delta_{pq} + 2r_{,p}r_{,q}r_{,k}\right] \\ &- \frac{1}{2\pi\mu r}(r_{,q}\delta_{pk} + r_{,p}\delta_{qk} + r_{,k}\delta_{pq} - 4r_{,p}r_{,q}r_{,k})\left(\frac{2\ell^2}{r^2} - K_2\left[\frac{r}{\ell}\right]\right) \\ &+ \frac{1}{4\pi\mu\ell}\left[r_{,q}\delta_{pk} + r_{,p}\delta_{qk} - 2r_{,p}r_{,q}r_{,k}\right]K_1\left[\frac{r}{\ell}\right], \end{aligned} \tag{11}$$

$$\Omega_k^{(\mathcal{F})} = \frac{e_{kp}r_{,p}}{4\pi\mu\ell}\left[\frac{\ell}{r} - K_1\left[\frac{r}{\ell}\right]\right], \tag{12}$$

where $\Omega_k^{(\mathcal{F})}$ is the rotation (in the x_3 direction) at point $\boldsymbol{x}$ due to a unit force acting in the kth direction.

Further, employing the constitutive and the balance equations, we derive the expressions for the stresses and the couple stresses as

$$\begin{aligned} \Sigma_{pqk}^{(\mathcal{F})} =& -\frac{1}{4\pi(1-\nu)r}\left[(1-2\nu)(r_{,q}\delta_{pk} + r_{,p}\delta_{qk} - r_{,k}\delta_{pq}) + 2r_{,p}r_{,q}r_{,k}\right] \\ &- \frac{1}{\pi r}(r_{,q}\delta_{pk} + r_{,p}\delta_{qk} + r_{,k}\delta_{pq} - 4r_{,p}r_{,q}r_{,k})\left(\frac{2\ell^2}{r^2} - K_2\left[\frac{r}{\ell}\right]\right) \\ &- \frac{1}{\pi\ell}\left[r_{,p}r_{,q}r_{,k} - r_{,q}\delta_{pk}\right]K_1\left[\frac{r}{\ell}\right], \end{aligned} \tag{13}$$

and

$$M_{qk}^{(\mathcal{F})} = \frac{e_{mk}}{\pi}r_{,m}r_{,q}\left(\frac{2\ell^2}{r^2} - K_2\left[\frac{r}{\ell}\right]\right) - \frac{e_{qk}}{\pi}\frac{\ell}{r}\left(\frac{\ell}{r} - K_1\left[\frac{r}{\ell}\right]\right). \tag{14}$$

Based on the asymptotic properties of the modified Bessel functions, we can readily deduce that the displacement (in the force direction) in couple stress elasticity retains the logarithmic singularity as $r \to 0$, just as in the case of classical elasticity. It is interesting to note, however, that for the special case of an incompressible material with $\nu = 0.5$, the displacement in couple stress elasticity becomes *bounded* since the logarithmic singularity is cancelled out by the logarithmic singularity arising from the Bessel function K_0 as $r \to 0$. Similarly, the strain and stress components remain singular and behave as $O(r^{-1})$ for $r \to 0$ in both theories, whereas the couple stresses exhibit a logarithmic singularity. However, in marked contrast with the classical theory, the rotation in couple stress elasticity is bounded at the point of application of the load. It is recalled that in the classical theory the rotation is singular, exhibiting an $O(r^{-1})$ variation as $r \to 0$. The above observations are summarized in Table 1.

Table 1
Asymptotic behaviour of the field quantities for the case of a concentrated force ($\mathcal{F}$).

	$\Sigma^{(\mathcal{F})}_{pqk}$	$M^{(\mathcal{F})}_{qk}$	$E^{(\mathcal{F})}_{pqk}$	$\Omega^{(\mathcal{F})}_{k}$	$U^{(\mathcal{F})}_{qk}$
Couple stress elasticity	$O(r^{-1})$	$O(\ln r)$	$O(r^{-1})$	$O(1)$	$O(\ln r)$
Classical elasticity	$O(r^{-1})$	–	$O(r^{-1})$	$O(r^{-1})$	$O(\ln r)$

Table 2
Asymptotic behaviour of the field quantities for the case of a concentrated couple.

	$\Sigma^{(\mathcal{M})}_{pq}$	$M^{(\mathcal{M})}_{q}$	$E^{(\mathcal{M})}_{pq}$	$\Omega^{(\mathcal{M})}$	$U^{(\mathcal{M})}_{q}$
Couple stress elasticity	$O(\ln r)$	$O(r^{-1})$	$O(1)$	$O(\ln r)$	$O(1)$

3.2. Concentrated couple

Consider now $u_q = U^{(\mathcal{M})}_q(\boldsymbol{x}, \boldsymbol{\xi})$, the component of the displacement in the qth direction at the point $\boldsymbol{x}$ caused by a unit couple ($\mathcal{M}$) in the x_3-direction at point $\boldsymbol{\xi}$. The displacement field in this case assumes the following form

$$U^{(\mathcal{M})}_q = \frac{e_{kq} r_{,k}}{4\pi\mu r}\left(1 - \frac{r}{\ell} K_1\left[\frac{r}{\ell}\right]\right), \tag{15}$$

and accordingly the strain tensor and the rotation become

$$E^{(\mathcal{M})}_{pq} = \frac{1}{8\pi\mu\ell^2}(e_{pk} r_{,q} r_{,k} + e_{qk} r_{,k} r_{,p})\left(\frac{2\ell^2}{r^2} - K_2\left[\frac{r}{\ell}\right]\right), \tag{16}$$

$$\Omega^{(\mathcal{M})} = \frac{1}{8\pi\mu\ell^2} K_0\left[\frac{r}{\ell}\right]. \tag{17}$$

The stresses and couple stresses read respectively

$$\Sigma^{(\mathcal{M})}_{pq} = \frac{1}{4\pi\ell^2}(e_{pk} r_{,q} r_{,k} + e_{qk} r_{,k} r_{,p})\left(\frac{2\ell^2}{r^2} - K_2\left[\frac{r}{\ell}\right]\right) - \frac{1}{4\pi\ell^2} e_{pq} K_0\left[\frac{r}{\ell}\right], \tag{18}$$

$$M^{(\mathcal{M})}_q = -\frac{r_{,q}}{2\pi\ell} K_1\left[\frac{r}{\ell}\right]. \tag{19}$$

Based on the asymptotic properties of the modified Bessel functions, we derive the asymptotic behaviour of the field quantities as $r \to 0$ which is summarized in Table 2. Note that the fundamental solution for a concentrated couple in the context of couple stress elasticity was given earlier by Weitsman [42] using a stress function approach.

It is worth noting that the same asymptotic behaviour for both fundamental solutions is also observed in micropolar elasticity under plane strain conditions [43], however, the detailed structure of the field quantities is different in the two theories. Also, we remark that the above fundamental solutions coincide with those obtained in [33,44] using a different approach.

4. Boundary integral formulation

The point of departure is the reciprocal theorem within the framework of couple stress elasticity [45]. Let $(u_q, \omega, t_q, \mathfrak{s}, X_q, Y)$ and $(u^*_q, \omega^*, t^*_q, \mathfrak{s}^*, X^*_q, Y^*)$ be two equilibrium states of the same two dimensional elastic body, then the reciprocal theorem states that

$$\int_\Gamma (t^*_q u_q - t_q u^*_q)\, d\Gamma + \int_\Gamma (\mathfrak{s}^* \omega - \mathfrak{s}\omega^*)\, d\Gamma + \int_\Omega (X^*_q u_q - X_q u^*_q)\, d\Omega + \int_\Omega (Y^* \omega - Y\omega^*)\, d\Omega = 0. \tag{20}$$

The Somigliana identities in couple stress theory can then be derived by using the reciprocal theorem (20) assuming that one of the equilibrium solutions coincides with the fundamental solution. Moreover, in what follows we also assume that the body forces and body couples vanish in the *actual* state, i.e. $X_q = 0$ and $Y = 0$, which is the case for the boundary value problems considered in this study.

For the case of the concentrated unit force ($\mathcal{F}$) we have that: $X_q^* = \delta_{qk}\delta(\boldsymbol{x}-\boldsymbol{\xi})\boldsymbol{e}_k$, $Y^* = 0$, and

$$u_q^* = U_{qk}^{(\mathcal{F})}(\boldsymbol{x},\boldsymbol{\xi})\boldsymbol{e}_k, \quad \omega^* = \Omega_k^{(\mathcal{F})}(\boldsymbol{x},\boldsymbol{\xi})\boldsymbol{e}_k, \quad t_q^* = T_{qk}^{(\mathcal{F})}(\boldsymbol{x},\boldsymbol{\xi})\boldsymbol{e}_k, \quad \mathfrak{s}^* = S_k^{(\mathcal{F})}(\boldsymbol{x},\boldsymbol{\xi})\boldsymbol{e}_k, \tag{21}$$

where $\delta(\boldsymbol{x})$ is the Dirac delta distribution, $T_{qk}^{(\mathcal{F})} = \Sigma_{pqk}^{(\mathcal{F})} n_p$ represents the force traction and $S_k^{(\mathcal{F})} = M_{pk}^{(\mathcal{F})} n_p$ represents the couple traction due to the concentrated force. In this case it can be readily shown that the first Somigliana identity for the displacements reads

$$u_k(\boldsymbol{\xi}) = \int_\Gamma U_{qk}^{(\mathcal{F})} t_q \, d\Gamma_x - \int_\Gamma T_{qk}^{(\mathcal{F})} u_q \, d\Gamma_x + \int_\Gamma \Omega_k^{(\mathcal{F})} \mathfrak{s} \, d\Gamma_x - \int_\Gamma S_k^{(\mathcal{F})} \omega \, d\Gamma_x, \tag{22}$$

with $\boldsymbol{\xi} \in \Omega \backslash \Gamma$, $\boldsymbol{x} \in \Gamma$, and $d\Gamma_x \equiv \Gamma(\boldsymbol{x})$.

For the case of the concentrated unit couple ($\mathcal{M}$) we have that: $X_q^* = 0$, $Y^* \equiv Y_3^* = \delta(\boldsymbol{x}-\boldsymbol{\xi})$, and

$$u_q^* = U_q^{(\mathcal{M})}(\boldsymbol{x},\boldsymbol{\xi}), \quad \omega^* = \Omega^{(\mathcal{M})}(\boldsymbol{x},\boldsymbol{\xi}), \quad t_q^* = T_q^{(\mathcal{M})}(\boldsymbol{x},\boldsymbol{\xi}), \quad \mathfrak{s}^* = S^{(\mathcal{M})}(\boldsymbol{x},\boldsymbol{\xi}). \tag{23}$$

where $T_q^{(\mathcal{M})} = \Sigma_{pq}^{(\mathcal{M})} n_p$ represents the force traction and $S^{(\mathcal{M})} = M_p^{(\mathcal{M})} n_p$ represents the couple traction due to a concentrated couple. In this case it can be readily shown that the second Somigliana identity for the rotation reads

$$\omega(\boldsymbol{\xi}) = \int_\Gamma U_q^{(\mathcal{M})} t_q \, d\Gamma_x - \int_\Gamma T_q^{(\mathcal{M})} u_q \, d\Gamma_x + \int_\Gamma \Omega^{(\mathcal{M})} \mathfrak{s} \, d\Gamma_x - \int_\Gamma S^{(\mathcal{M})} \omega \, d\Gamma_x \tag{24}$$

with $\boldsymbol{\xi} \in \Omega \backslash \Gamma$ and $\boldsymbol{x} \in \Gamma$. It is worth noting that the second Somigliana identity (24) can be obtained directly from the first one by applying the curl operator ($(1/2)e_{pq}\partial_p$) to Eq. (22). This is due to the fact that in couple stress elasticity the rotation is constrained with the displacement through Eq. (3). On the contrary, in micropolar theory both integral equations are independent [25]. Finally, we note that the internal stresses and internal couple stresses can be derived by combining the derivatives of (22) in conjunction with Eqs (2) and (3) to produce the strain and curvature components and then using the constitutive Eqs. (5)–(6) together with Eq. (7). Expressions for the internal stress and couple stresses can be found in [34].

Following the limiting process proposed by Liang and Huang [25] in micropolar elasticity, we let $\boldsymbol{\xi} \to \Gamma$ in Eqs (22) and (24). Two boundary integral equations are then derived, a vector equation for the displacements (DBIE) and a scalar equation for the out-of-plane rotation, which we call a rotation boundary integral equation (RBIE). The boundary integral equations assume the following form (with the dependence of the Green's functions and field quantities on the field and source points omitted for brevity):

$$c_{qk}\, u_q + \cancel{\int_\Gamma} T_{qk}^{(\mathcal{F})} u_q \, d\Gamma_x + \int_\Gamma S_k^{(\mathcal{F})} \omega \, d\Gamma_x = \int_\Gamma U_{qk}^{(\mathcal{F})} t_q \, d\Gamma_x + \int_\Gamma \Omega_k^{(\mathcal{F})} \mathfrak{s} \, d\Gamma_x, \tag{25}$$

$$c_o\, \omega + \int_\Gamma T_q^{(\mathcal{M})} u_q \, d\Gamma_x + \cancel{\int_\Gamma} S^{(\mathcal{M})} \omega \, d\Gamma_x = \int_\Gamma U_q^{(\mathcal{M})} t_q \, d\Gamma_x + \int_\Gamma \Omega^{(\mathcal{M})} \mathfrak{s} \, d\Gamma_x. \tag{26}$$

where $\cancel{\int}$ denotes that the integral is interpreted in the Cauchy principal value (CPV) sense. The free terms $c_{qk}(\boldsymbol{\xi})$ and $c_o(\boldsymbol{\xi})$ can be obtained by using the concept of a rigid body motion. Analytical expressions of the free terms in couple stress elasticity for the general case of a non-smooth boundary are presented in Appendix B. For the case of a smooth boundary it is shown that $c_{pq} = (1/2)\delta_{pq}$ as in the classical theory, and $c_o = 1/2$.

5. Isogeometric formulation

The traditional development of the Boundary Element Method involves the discretization of a Boundary Integral Equation, so that boundary Γ is subdivided into non-overlapping elements, i.e. $\Gamma = \cup_{i=1}^{n_e} \Gamma_i$, over each of which the solution variables are assumed to vary in a prescribed way. The classical development is to write, for example, the displacement in the qth direction in a piecewise polynomial expansion,

$$u_q(\eta) = \sum_{\alpha=1}^{J} N_\alpha(\eta) u_q^\alpha, \tag{27}$$

where u_q^α is the displacement in the qth direction at node α of J on an element, N_α is the polynomial shape function for the node α, and $\eta \in (-1, 1)$ is the parametric coordinate defining the element. The main idea behind isogeometric formulations is, for the descriptions of both the geometry and the solution variables, to replace the use

of polynomial shape functions with basis functions underlying Non-Uniform Rational B-Splines (NURBS). Thus, the displacement expansion becomes

$$u_q(\phi) = \sum_{\alpha=0}^{n_c-1} R_{\alpha,p}(\phi) A_q^\alpha, \tag{28}$$

where $R_{\alpha,p}(\phi)$ is the NURBS basis function for control point α, n_c is the number of control points, p is the degree of the NURBS spline and ϕ is the parametric coordinate used in the spline definition. We denote using A_q^α a set of coefficients that, once they become known through the IGABEM solution, will allow the displacement to be fully recovered by application of (28). While it plays a role similar to the nodal displacement u_q^α in (27), A_q^α should not be thought of as a nodal displacement because (i) the concept of nodes is lost in moving to isogeometric formulations, and (ii) the basis functions $R_{\alpha,p}(\phi)$ are non-interpolatory. It should also be noted that the notation for NURBS basis functions, $R_{\alpha,p}$, is standard and the comma should not be interpreted as indicating differentiation.

Similarly to (28), one can write the traction components t_q, rotation ω and couple-traction, $\mathfrak{s}$, in expansions of the NURBS basis functions,

$$t_q(\phi) = \sum_{\alpha=0}^{n_c-1} R_{\alpha,p}(\phi) B_q^\alpha, \tag{29}$$

$$\omega(\phi) = \sum_{\alpha=0}^{n_c-1} R_{\alpha,p}(\phi) D^\alpha, \tag{30}$$

$$\mathfrak{s}(\phi) = \sum_{\alpha=0}^{n_c-1} R_{\alpha,p}(\phi) E^\alpha, \tag{31}$$

with B_q^α, D^α and E^α becoming unknown coefficients alongside A_q^α. The construction of NURBS basis functions and splines is standard and will be presented here only briefly; the interested reader is directed to Piegl & Tiller's classic text [46]. The starting point is the knot vector Φ, containing a non-decreasing set of n_k numbers (the knots) in the parametric variable ϕ, i.e.

$$\Phi = \{\phi_0, \phi_1, \ldots, \phi_{n_k-1}\}. \tag{32}$$

The B-spline basis functions are then constructed using the Cox–de Boor recursive relations, starting with degree $p = 0$:

$$N_{\alpha,0}(\phi) = \begin{cases} 1 \text{if } \phi_\alpha \le \phi \le \phi_{\alpha+1} \\ 0 \qquad\qquad \text{otherwise} \end{cases}, \tag{33}$$

and then, recursively, for higher degree

$$N_{\alpha,p}(\phi) = \frac{\phi - \phi_\alpha}{\phi_{\alpha+p} - \phi_\alpha} N_{\alpha,p-1}(\phi) + \frac{\phi_{\alpha+p+1} - \phi}{\phi_{\alpha+p+1} - \phi_{\alpha+1}} N_{\alpha+1,p-1}(\phi). \tag{34}$$

The number of control points, n_c, and the number of knots, n_k, are linked by the relation $n_c = n_k - p - 1$. Finally, the NURBS basis functions may be found by applying a set of weights w_α to the B-spline basis functions,

$$R_{\alpha,p}(\phi) = \frac{N_{\alpha,p}(\phi) w_\alpha}{\sum_{\beta=0}^{n_c-1} N_{\beta,p}(\phi) w_\beta}, \qquad (\alpha \text{ not summed}). \tag{35}$$

A NURBS curve $C(\phi)$ may now be formed from the above basis functions and a set of control points $P_\alpha \in \mathbb{R}^2$, using

$$C(\phi) = \sum_{\alpha=0}^{n_c-1} R_{\alpha,p}(\phi) P_\alpha. \tag{36}$$

In a wide body of literature on isogeometric methods, the set of NURBS basis functions has been consistently shown to offer some key benefits: (i) the NURBS spline (36) can exactly reproduce conic sections, (ii) the NURBS definition facilitates a direct linkage between CAD and analysis, and (iii) the smoothness and non-negativity of

the basis offer improved convergence properties in finite element and boundary element approximations (see, for example in an IGABEM context, [47]).

Substitution of the NURBS expansions for the solution variables, (28) to (31), into the boundary integral Eqs. (25) and (26), yields a discretized form

$$c_{qk}(\boldsymbol{\xi})u_q(\boldsymbol{\xi}) + \sum_{\alpha=0}^{n_c-1}\left[\mathfrak{R}^{(\mathcal{F})}_{\alpha qk}A^{\alpha}_{q} + \mathfrak{L}^{(\mathcal{F})}_{\alpha k}D^{\alpha}\right] = \sum_{\alpha=0}^{n_c-1}\left[\mathfrak{D}^{(\mathcal{F})}_{\alpha qk}B^{\alpha}_{q} + \mathfrak{M}^{(\mathcal{F})}_{\alpha k}E^{\alpha}\right] \tag{37}$$

$$c_{o}(\boldsymbol{\xi})\omega(\boldsymbol{\xi}) + \sum_{\alpha=0}^{n_c-1}\left[\mathfrak{R}^{(\mathcal{M})}_{\alpha q}A^{\alpha}_{q} + \mathfrak{L}^{(\mathcal{M})}_{\alpha}D^{\alpha}\right] = \sum_{\alpha=0}^{n_c-1}\left[\mathfrak{D}^{(\mathcal{M})}_{\alpha q}B^{\alpha}_{q} + \mathfrak{M}^{(\mathcal{M})}_{\alpha}E^{\alpha}\right] \tag{38}$$

where

$$\mathfrak{R}^{(\mathcal{F})}_{\alpha qk} = \int_{\Gamma} R_{\alpha,p}(\phi(\boldsymbol{x}))T^{(\mathcal{F})}_{qk}(\boldsymbol{x},\boldsymbol{\xi})d\Gamma_x, \tag{39}$$

$$\mathfrak{L}^{(\mathcal{F})}_{\alpha k} = \int_{\Gamma} R_{\alpha,p}(\phi(\boldsymbol{x}))S^{(\mathcal{F})}_{k}(\boldsymbol{x},\boldsymbol{\xi})d\Gamma_x, \tag{40}$$

$$\mathfrak{D}^{(\mathcal{F})}_{\alpha qk} = \int_{\Gamma} R_{\alpha,p}(\phi(\boldsymbol{x}))U^{(\mathcal{F})}_{qk}(\boldsymbol{x},\boldsymbol{\xi})d\Gamma_x, \tag{41}$$

$$\mathfrak{M}^{(\mathcal{F})}_{\alpha k} = \int_{\Gamma} R_{\alpha,p}(\phi(\boldsymbol{x}))\Omega^{(\mathcal{F})}_{k}(\boldsymbol{x},\boldsymbol{\xi})d\Gamma_x, \tag{42}$$

$$\mathfrak{R}^{(\mathcal{M})}_{\alpha q} = \int_{\Gamma} R_{\alpha,p}(\phi(\boldsymbol{x}))T^{(\mathcal{M})}_{q}(\boldsymbol{x},\boldsymbol{\xi})d\Gamma_x, \tag{43}$$

$$\mathfrak{L}^{(\mathcal{M})}_{\alpha} = \int_{\Gamma} R_{\alpha,p}(\phi(\boldsymbol{x}))S^{(\mathcal{M})}(\boldsymbol{x},\boldsymbol{\xi})d\Gamma_x, \tag{44}$$

$$\mathfrak{D}^{(\mathcal{M})}_{\alpha q} = \int_{\Gamma} R_{\alpha,p}(\phi(\boldsymbol{x}))U^{(\mathcal{M})}_{q}(\boldsymbol{x},\boldsymbol{\xi})d\Gamma_x, \tag{45}$$

$$\mathfrak{M}^{(\mathcal{M})}_{\alpha} = \int_{\Gamma} R_{\alpha,p}(\phi(\boldsymbol{x}))\Omega^{(\mathcal{M})}(\boldsymbol{x},\boldsymbol{\xi})d\Gamma_x. \tag{46}$$

The above boundary integrals may be evaluated element-by-element, noting that in IGABEM the concept of an 'element' can usefully be interpreted as a knot-span, i.e. the interval between unique knots in the knot vector Φ. We collocate Eqs. (37) and (38) at a number of collocation points that equals the number of control points. Here, again, the IGABEM implementation necessarily differs from conventional BEM, in that the control points cannot themselves be used as collocation points because they do not in general lie on the boundary Γ. It is common in IGABEM to collocate at the so-called Greville abscissae [48], and we adopt this approach in the current work.

Application of boundary conditions in the conventional BEM fashion yields a square linear system of equations in unknowns $\{(A^{\alpha}_{q}, B^{\alpha}_{q}, D^{\alpha}, E^{\alpha}), \alpha = 0, \ldots, n_c - 1, q = (1, 2)\}$ that can readily be solved. Boundary displacements, tractions, rotations and couple-tractions can then be recovered by application of Eqs. (28) to (31).

6. An analytical couple stress solution for the elliptical hole problem

An analytical solution is derived here for the plane strain problem of an elliptical hole in an infinite plate under uniform tension in couple stress elasticity. Previous works dealing with the elliptical openings in couple stress theory include the work by Hsu et al. [49] where an approach based on Mathieu functions was employed and a set of approximate boundary conditions was used satisfying the traction free conditions on the hole only in an average sense. No results were presented in this work. Itou [50] employed the Schimdt method in conjunction with a polar coordinates formulation showing some results for the stress concentration factor (SCF) in the form of graphs. However, the method employed there works well only for ratios of the major to minor axis of the ellipse that are close to unity. Recently, Haftbaradaran and Shodja [51] have examined elliptic inhomogeneities and inclusion problems in antiplane couple stress elasticity. Our approach is based on Mathieu functions and a modified version of the Schmidt method [50,52,53]. Note that summation convention is *not* employed in this Section.

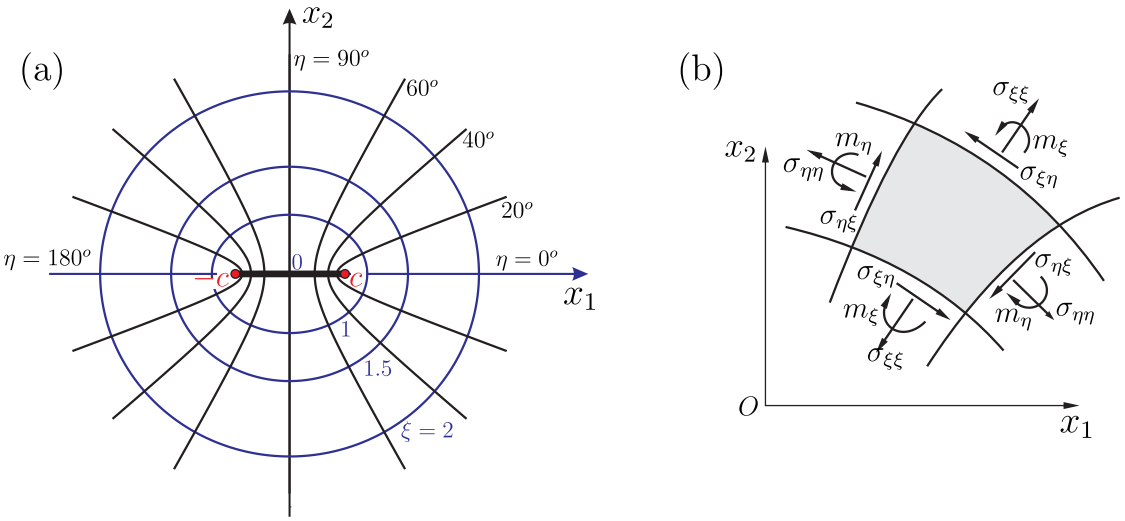

Fig. 1. (a) Elliptic coordinates system (b) Positive components of stress and couple stress components in elliptic coordinates.

We work with elliptic coordinates (ξ, η) which are related with (x_1, x_2) through the expressions

$$x_1 = c\cosh\xi\,\cos\eta \quad \text{and} \quad x_2 = c\sinh\xi\,\sin\eta, \tag{47}$$

where $0 \le \xi \le \infty$ and $0 \le \eta \le 2\pi$. The curves $\xi = const.$ and $\eta = const.$ constitute an orthogonal curvilinear system of hyperbolas and confocal ellipses, respectively, with common foci the points at $(\pm c, 0)$, as shown in Fig. 1(a). Also, in Fig. 1(b) the positive components of the in-plane stress and couple stresses are shown in the elliptic coordinate system.

Mindlin [54] showed that the stresses and couple stresses can be expressed in terms of two stress functions that satisfy the equilibrium Eqs. (4) (with zero body force and body couple) automatically. In elliptic coordinates, the relations between the Mindlin's stress functions $\Phi(\xi, \eta)$ and $\Psi(\xi, \eta)$ and the stress and couple stress components assume the following form [49]

$$\begin{aligned}\sigma_{\xi\xi} =& \frac{2}{c^2\mathcal{A}}\frac{\partial^2\Phi}{\partial\eta^2} + \frac{2}{c^2\mathcal{A}^2}\sinh 2\xi\,\frac{\partial\Phi}{\partial\xi} - \frac{2}{c^2\mathcal{A}^2}\sin 2\eta\,\frac{\partial\Phi}{\partial\eta} - \frac{2}{c^2\mathcal{A}}\frac{\partial^2\Psi}{\partial\xi\,\partial\eta}\\ &+ \frac{2}{c^2\mathcal{A}^2}\sin 2\eta\,\frac{\partial\Psi}{\partial\xi} + \frac{2}{c^2\mathcal{A}^2}\sinh 2\xi\,\frac{\partial\Psi}{\partial\eta},\end{aligned} \tag{48}$$

$$\begin{aligned}\sigma_{\eta\eta} =& \frac{2}{c^2\mathcal{A}}\frac{\partial^2\Phi}{\partial\xi^2} - \frac{2}{c^2\mathcal{A}^2}\sinh 2\xi\,\frac{\partial\Phi}{\partial\xi} + \frac{2}{c^2\mathcal{A}^2}\sin 2\eta\,\frac{\partial\Phi}{\partial\eta} + \frac{2}{c^2\mathcal{A}}\frac{\partial^2\Psi}{\partial\xi\,\partial\eta}\\ &- \frac{2}{c^2\mathcal{A}^2}\sin 2\eta\,\frac{\partial\Psi}{\partial\xi} - \frac{2}{c^2\mathcal{A}^2}\sinh 2\xi\,\frac{\partial\Psi}{\partial\eta},\end{aligned} \tag{49}$$

$$\begin{aligned}\sigma_{\xi\eta} =& -\frac{2}{c^2\mathcal{A}}\frac{\partial^2\Phi}{\partial\xi\,\partial\eta} + \frac{2}{c^2\mathcal{A}^2}\sin 2\eta\,\frac{\partial\Phi}{\partial\xi} + \frac{2}{c^2\mathcal{A}^2}\sinh 2\xi\,\frac{\partial\Phi}{\partial\eta} - \frac{2}{c^2\mathcal{A}}\frac{\partial^2\Psi}{\partial\eta^2}\\ &- \frac{2}{c^2\mathcal{A}^2}\sinh 2\xi\,\frac{\partial\Psi}{\partial\xi} + \frac{2}{c^2\mathcal{A}^2}\sin 2\eta\,\frac{\partial\Psi}{\partial\eta},\end{aligned} \tag{50}$$

$$\sigma_{\eta\xi} = \sigma_{\xi\eta} + \nabla^2\Psi, \tag{51}$$

$$m_\xi = \frac{\sqrt{2}}{c\sqrt{\mathcal{A}}}\frac{\partial\Psi}{\partial\xi}, \quad m_\eta = \frac{\sqrt{2}}{c\sqrt{\mathcal{A}}}\frac{\partial\Psi}{\partial\eta}, \tag{52}$$

where

$$\mathcal{A} = \cosh 2\xi - \cos 2\eta \quad \text{and} \quad \nabla^2 = \frac{2}{c^2\mathcal{A}}\left[\frac{\partial^2}{\partial\xi^2} + \frac{\partial^2}{\partial\eta^2}\right]. \tag{53}$$

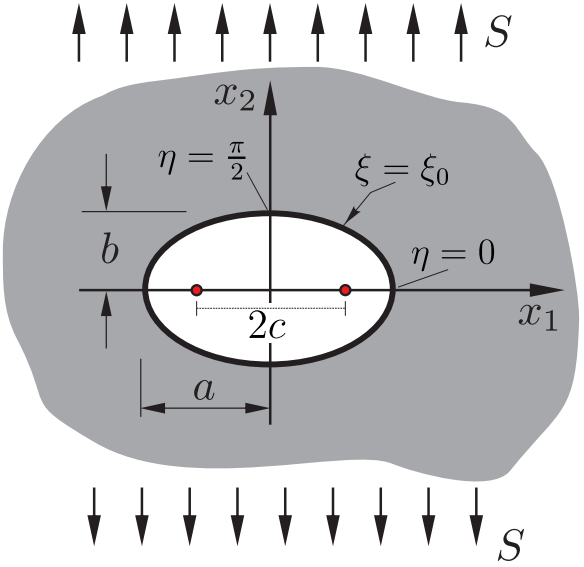

Fig. 2. Elliptic hole in an infinite planar domain under uniform tension perpendicular to the major axis of the ellipse.

Compatibility requires that the stress functions in couple stress elasticity satisfy a coupled system of differential equations [54] which in elliptic coordinates assumes the following form

$$\partial_\xi(\Psi - \ell^2\nabla^2\Psi) = -2(1-\nu)\ell^2\partial_\eta(\nabla^2\Phi) \quad \text{and} \quad \partial_\eta(\Psi - \ell^2\nabla^2\Psi) = 2(1-\nu)\ell^2\partial_\xi(\nabla^2\Phi), \tag{54}$$

which in turn implies that

$$\nabla^4\Phi = 0 \quad \text{and} \quad \nabla^2\Psi - \ell^2\nabla^4\Psi = 0. \tag{55}$$

The solution of $(55)_1$, taking into account also the symmetries for the stresses in our boundary value problem (see Fig. 2), is expressed as [55]

$$\begin{aligned}\Phi =& w_1\xi + \sum_{m=1}^{\infty} w_{m+1}e^{-2\ m\xi}\cos 2m\eta + \sum_{m=1}^{\infty} p_m e^{2\ m\xi}\cos 2m\eta \\ &+ \sum_{m=1}^{\infty} f_m\Big(e^{-(2m-2)\xi}\cos 2\ m\eta + e^{-2m\xi}\cos(2m-2)\eta\Big) \\ &+ \sum_{m=1}^{\infty} d_m\Big(e^{(2m-2)\xi}\cos 2\ m\eta + e^{2m\xi}\cos(2m-2)\eta\Big)\end{aligned} \tag{56}$$

where we note that first three terms on the RHS of (56) are harmonic while the rest of them are biharmonic. The general solution of $(55)_2$ can be expressed as $\Psi = \Psi_0 + \Psi_1$ where the functions $\Psi_0(\xi,\eta)$ and $\Psi_1(\xi,\eta)$ are the solutions of the partial differential equations

$$\nabla^2\Psi_0 = 0 \quad \text{and} \quad \Psi_1 - \ell^2\nabla^2\Psi_1 = 0. \tag{57}$$

Note that the compatibility Eqs. (54) in conjunction with (57) imply that the functions Ψ_0 and $-2(1-\nu)\ell^2\nabla^2\Phi$ must be harmonic conjugates. This leads to the following form for Ψ_0

$$\Psi_0 = \sum_{m=1}^{\infty}\frac{h_m}{\mathcal{A}}\Big(e^{-(2m-2)\xi}\sin 2\ m\eta - e^{-2m\xi}\sin(2m-2)\eta\Big). \tag{58}$$

Finally, for the solution of $(57)_2$ we take (see McLachlan [56], p.311, and [57])

$$\Psi_1 = \sum_{m=1}^{\infty} g_m\frac{Gek_{2m}[\xi,-q]}{Gek_{2m}[\xi_0,-q]}se_{2m}[\eta,-q] \tag{59}$$

where $q = c^2/(4\ell^2)$, Gek_{2m} is the modified Mathieu function of the second kind of the $2m$ order, and se_{2m} is the first kind angular Mathieu function with odd parity[1]. The Mathieu functions are defined as [56]

$$se_{2m}[\eta, -q] = (-1)^{m-1} \sum_{j=0}^{N} (-1)^j B_{2j+2}^{(2\ m)} \sin(2j+2)\eta, \tag{60}$$

$$Gek_{2m}[\xi, -q] = (-1)^m \frac{\hat{s}_{2m}}{\pi B_2^{(2\ m)}} \sum_{j=0}^{N} B_{2j+2}^{(2\ m)} \Big(I_j[\chi_1] K_{j+2}[\chi_2] - I_{j+2}[\chi_1] K_j[\chi_2] \Big), \tag{61}$$

with $\chi_1 = \sqrt{q} e^{-\xi}$, $\chi_2 = \sqrt{q} e^{\xi}$, and $\hat{s}_{2m} = \left\{ se'_{2m}(0,q) \cdot se'_{2m}(\pi/2, q) \right\} / \left\{ q B_2^{(2\ m)} \right\}$. The prime denotes differentiation with respect to the variable η, and $I_j[\cdot]$ is the modified Bessel function of the first kind. The coefficients B_j in the above relations are functions of q and the characteristic number and they are evaluated by employing the pertinent recurrence relations for se_{2m} (see Chapter 3 in [56]). It is worth noting that the above product series representation of Gek_{2m} converges absolutely and uniformly for all values ξ, and rapid convergence is observed for small and moderate values of q and m [56]. In the limiting case where the ellipse tends to a circle, the eccentricity goes to zero and thus $c \to 0$ and accordingly $q \to 0$. The Mathieu functions can be then represented by their simpler forms ([56], pp. 367–369)

$$se_{2m}[\eta, -q] \to \sin 2m\eta, \quad \text{and} \quad Gek_{2m}[\xi, -q] \to (-1)^m \pi^{-1} \hat{s}_{2m} K_{2m}[\sqrt{q} e^{\xi}], \tag{62}$$

which become useful in the numerical computations when the elliptical boundary of the hole tends to a circle.

Fig. 2 depicts an elliptical hole in an infinite domain under plane strain conditions where the far field loading S is normal to the major semi-axis a of the ellipse. The boundary of the elliptical hole is defined by $\xi = \xi_0$ and its foci at $(\pm c, 0)$ with $c = (a^2 - b^2)^{1/2}$ and b being the minor semi-axis of the ellipse ($b \le a$).

The boundary conditions at the elliptical hole are

$$\sigma_{\xi\xi}(\xi_0, \eta) = 0, \qquad \sigma_{\xi\eta}(\xi_0, \eta) = 0, \qquad m_{\xi}(\xi_0, \eta) = 0, \tag{63}$$

whereas the regularity conditions at infinity are

$$\sigma_{22}^{\infty} = S, \quad \sigma_{11}^{\infty} = \sigma_{12}^{\infty} = \sigma_{21}^{\infty} = m_1^{\infty} = m_2^{\infty} = 0, \tag{64}$$

as $x_1^2 + x_2^2 \to \infty$. Employing the regularity conditions and using the compatibility Eqs. (54), we readily derive that

$$p_m = \begin{cases} \frac{Sc^2}{16}, & m = 1, \\ 0, & m > 1, \end{cases} \quad d_m = \begin{cases} \frac{Sc^2}{16}, & m = 1, \\ 0, & m > 1, \end{cases} \quad f_m = \begin{cases} \frac{Sc^2}{16} + \frac{q\, h_1}{4(1-\nu)}, & m = 1, \\ \frac{q\, h_m}{4(1-\nu)(2m-1)}, & m > 1, \end{cases} \tag{65}$$

The stress functions for the elliptical hole problem become finally

$$\begin{aligned} \Phi =& \frac{Sc^2}{16} \left(2\cos 2\eta + e^{2\xi} + e^{-2\xi} + e^{2\xi} \cos 2\eta \right) + w_1 \xi + \sum_{m=1}^{\infty} w_{m+1} e^{-2\ m\xi} \cos 2m\eta \\ &+ \frac{q}{4(1-\nu)} \sum_{m=1}^{\infty} \frac{h_m}{2m-1} \Big(e^{-(2m-2)\xi} \cos 2\ m\eta + e^{-2m\xi} \cos (2m-2)\eta \Big), \end{aligned} \tag{66}$$

$$\Psi = \sum_{m=1}^{\infty} \frac{h_m}{\mathcal{A}} \Big(e^{-(2m-2)\xi} \sin 2\ m\eta - e^{-2m\xi} \sin (2m-2)\eta \Big) + \sum_{m=1}^{\infty} g_m \frac{Gek_{2m}[\xi, -q]}{Gek_{2m}[\xi_0, -q]} se_{2m}[\eta, -q]. \tag{67}$$

The stresses and couple stresses can then be derived using Eqs (48)–(53). Truncating the series solution, the boundary conditions (63) can now be written in the following form [50]

$$\sum_{m=1}^{M} \Big[w_m \mathcal{W}_m^{(\sigma)}(\eta) + h_m \mathcal{H}_m^{(\sigma)}(\eta) + g_m \mathcal{G}_m^{(\sigma)}(\eta) \Big] = -s(\eta), \tag{68}$$

$$\sum_{m=1}^{M} \Big[w_m \mathcal{W}_m^{(\tau)}(\eta) + h_m \mathcal{H}_m^{(\tau)}(\eta) + g_m \mathcal{G}_m^{(\tau)}(\eta) \Big] = -\tau(\eta), \tag{69}$$

[1] Note that in Hsu et al. [49] in the solution for Ψ_1, the modified Mathieu function Fek_{2m} was erroneously used instead of Gek_{2m}.

Table 3
Convergence of SCF for the analytical series solution.
The Poisson's ratio is $\nu = 0.25$ and $a/\ell = 10$.

	SCF			
M	$b/a = 1$	$b/a = 0.5$	$b/a = 0.25$	$b/a = 0.15$
10	4.32791	4.32791	6.51968	9.00925
12	·	4.32766	6.53859	9.10058
14	·	4.32763	6.54244	9.14402
16	·	·	6.54339	9.20276
18	·	·	6.54365	9.23133
20	·	·	6.54372	9.23950
22	·	·	6.54374	9.24156
24	·	·	6.54376	9.24203
26	·	·	·	9.24211
28	·	·	·	9.24209

$$\sum_{m=1}^{M}\Big[h_m \mathcal{H}_m^{(\mu)}(\eta) + g_m\, \mathcal{G}_m^{(\mu)}(\eta)\Big] = 0, \tag{70}$$

with

$$\begin{cases} s(\eta) = \frac{S}{8\mathcal{A}_0^2}\Big(\mathcal{A}_0\big(1 - e^{4\xi_0} + 2\mathcal{A}_0(2 + e^{2\xi_0})\big) + 2\sinh 2\xi_0\Big) \\ \tau(\eta) = \frac{S}{4}\frac{\sin 2\eta}{\mathcal{A}_0^2}\left(1 + \mathcal{A}_0 e^{2\xi_0}\right), \end{cases} \qquad \mathcal{A}_0 = \cosh 2\xi_0 - \cos 2\eta \tag{71}$$

and

$$\begin{aligned} &\mathcal{W}_m^{(\sigma)}(\eta) = \partial_{w_m}\sigma_{\xi\xi}(\xi_0,\eta), \quad \mathcal{H}_m^{(\sigma)}(\eta) = \partial_{h_m}\sigma_{\xi\xi}(\xi_0,\eta), \quad \mathcal{G}_m^{(\sigma)}(\eta) = \partial_{g_m}\sigma_{\xi\xi}(\xi_0,\eta), \\ &\mathcal{W}_m^{(\tau)}(\eta) = \partial_{w_m}\sigma_{\xi\eta}(\xi_0,\eta), \quad \mathcal{H}_m^{(\tau)}(\eta) = \partial_{h_m}\sigma_{\xi\eta}(\xi_0,\eta), \quad \mathcal{G}_m^{(\tau)}(\eta) = \partial_{g_m}\sigma_{\xi\eta}(\xi_0,\eta), \\ &\mathcal{H}_m^{(\mu)}(\eta) = \partial_{h_m} m_{\xi}(\xi_0,\eta), \quad \mathcal{G}_m^{(\mu)}(\eta) = \partial_{g_m} m_{\xi}(\xi_0,\eta), \quad m \geq 1. \end{aligned} \tag{72}$$

The explicit expressions of the above functions are lengthy and are not shown here. The solution of the system of Eqs. (68)–(70) is achieved by using the modified Schmidt orthogonalization process as described in [50,52]. The procedure is detailed in Appendix C. Once the coefficients w_m, h_m and g_m are known, the stress functions can be evaluated from (66) and (67) and accordingly the stresses and couple stresses from (48)–(53).

The accuracy of the solution depends on M: the number of terms in the series solution, and N: the number of terms to compute the Mathieu functions in (60) and (61). It is found that $N = M + 5$ works well for the evaluation of the Mathieu functions of order $2M$ and for small and moderate values of q. Note that as the ratios b/a and ℓ/a decrease, a larger M is required for a converged solution. Table 3 shows the convergence of the series solution for the stress concentration factor (SCF) K_t as computed from (75) for a couple stress material with Poisson's ratio $\nu = 0.25$ and $a/\ell = 10$.

7. Application examples

In this section, we consider a number of examples which illustrate various features of the numerical behaviour of the solutions. In all examples, a consistent set of units is used with null couple stress boundary conditions applied at all boundaries.

7.1. Circular hole in infinite plate

We study a plane strain problem of a circular hole of radius a in a large domain under an applied far-field biaxial tensile stress of $\bar{\sigma}_1$ and $\bar{\sigma}_2$ ($\bar{\sigma}_1 > \bar{\sigma}_2$) in the x_1 and x_2 directions, respectively. Mindlin [54] provides the analytical solution for the maximum circumferential stress on the rim of the circular opening as

$$\sigma_{max} = \frac{3\bar{\sigma}_1 - \bar{\sigma}_2 + (\bar{\sigma}_1 + \bar{\sigma}_2)F}{1 + F} \tag{73}$$

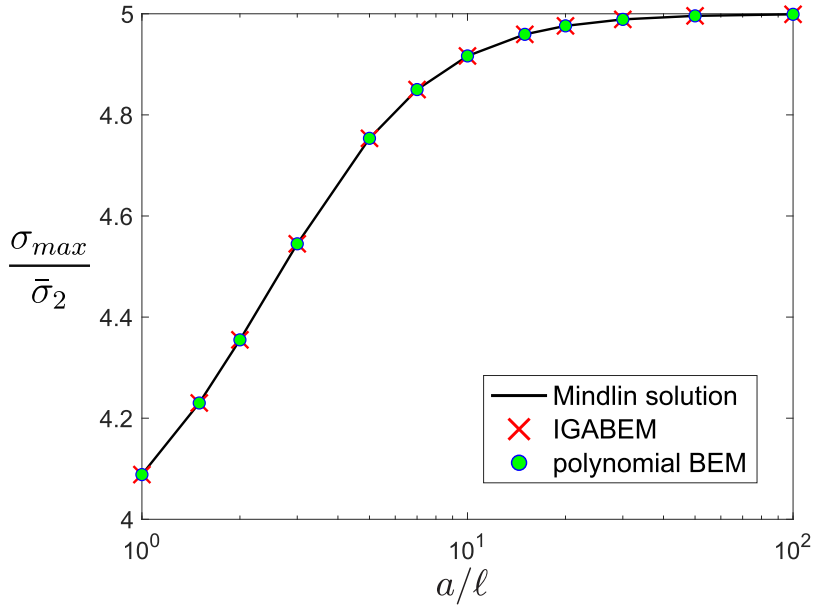

Fig. 3. Maximum stress at rim of the circular hole under biaxial loading as a function of a/ℓ.

where

$$F = \frac{8(1-\nu)}{4 + \frac{a^2}{\ell^2} + \frac{2a}{\ell}\frac{K_0[a/\ell]}{K_1[a/\ell]}}, \tag{74}$$

We consider a material having Poisson's ratio $\nu = 0.33$, with the plate subjected to far field stresses $\bar{\sigma}_1 = 2\bar{\sigma}_2$. For the purposes of analysis the infinite domain is truncated by a large square box. Since the meshing is confined to the boundary, we can use an arbitrarily large square without incurring the cost of more elements, and in our analyses we define a square of side $10^6 a$.

Fig. 3 shows the variation of maximum stress with a/ℓ. For these results we use 64 elements to discretize the circular hole. The IGABEM solution is derived from a model containing 64 elements (i.e. knot spans) on the circular hole, with NURBS basis functions of degree $p = 2$. The results are compared against a conventional BEM scheme using 64 piecewise-quadratic elements to model the circular hole. It is evident that both polynomial BEM and IGABEM formulations produce results that correlate well against the analytical solution.

7.1.1. Convergence

Fig. 4 displays the convergence of the two formulations for ratios $a/\ell = \{1.5, 15, 50\}$, respectively. The plots show that the IGABEM outperforms polynomial BEM offering up to one order of magnitude reduction in error. As in most isogeometric implementations, the improved accuracy can be attributed to a combination of two factors: the smoother, non-negative basis functions and the higher fidelity representation of the geometry. Recalling that conic sections may be represented exactly using NURBS, it follows that for this example of a circular hole the geometry of the circle is represented exactly in the IGABEM scheme, while some geometric errors are made using the quadratic element. This effect will be most evident in the coarser meshes and it can consequently be seen that for some a/ℓ (e.g. the case $a/\ell = 50$ in Fig. 4c) the benefit of IGABEM becomes less pronounced for the finer discretizations.

In Fig. 4 the lines showing the convergence rate for IGABEM have been calculated by neglecting the point relating to the coarsest mesh (ndof = 72, displayed on the left edge of the plot). It is interesting to see the surprisingly good performance of the coarsest IGABEM model consistently providing results of better accuracy than the next refinement level (ndof = 108). The reason for this curiously beneficial preasymptotic behaviour is unclear. The convergence rates of the polynomial and IGABEM formulations are similar, with IGABEM generally exhibiting a slightly higher convergence rate for moderate a/ℓ, but with the polynomial basis converging more rapidly for large a/ℓ as the solution approaches that for classical elasticity.

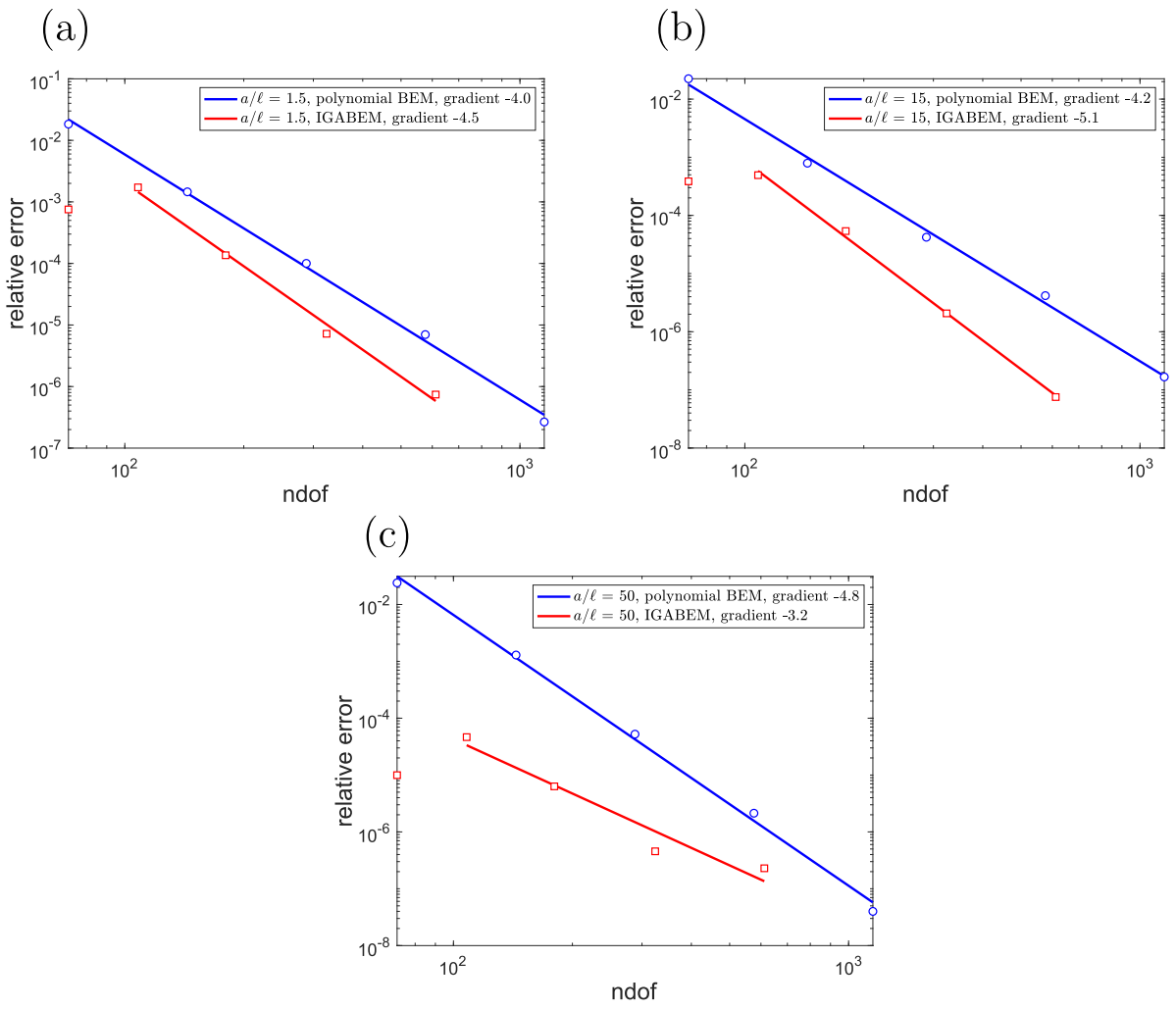

Fig. 4. Convergence for circular opening, (a) $a/\ell = 1.5$, (b) $a/\ell = 15$, (c) $a/\ell = 50$.

7.2. Elliptical openings

The next case is that of an elliptical hole in an infinite domain under the action of a uniaxial far-field stress S normal to the major axis of the ellipse as shown in Fig. 2. The analytical plane strain solution was derived in Section 6. The problem was examined using the standard BEM in the recent work of Lei et al. [33]. In Fig. 5 we present the variation of the stress concentration factor, K_t, with the ratio a/ℓ for a material with Poisson's ratio $\nu = 0.25$. Here we use a conventional definition of the stress concentration factor, in terms of the maximum circumferential stress σ_{max}, as

$$K_t = \frac{\sigma_{max}}{S} \tag{75}$$

In the figure, the results of a refined IGABEM scheme with 1620 degrees of freedom are presented for ellipse aspect ratios $b/a = \{1, 0.5, 0.25\}$, with the first of these representing a circular hole. The IGABEM results compare very well with the analytical solution and are seen to converge towards the famous classical solution due to Inglis [58] i.e. $K_t = \{3, 5, 9\}$ (respectively), for large a/ℓ as we move towards classical elasticity. We note that the convergence to the classical solution is slower for ellipses with more extreme aspect ratio, so that even for $a/\ell = 100$, the stress concentration factor for the case $b/a = 0.25$ is $K_t = 8.59$, i.e. 4.6% lower than the asymptotic value of $K_t = 9$ for this aspect ratio.

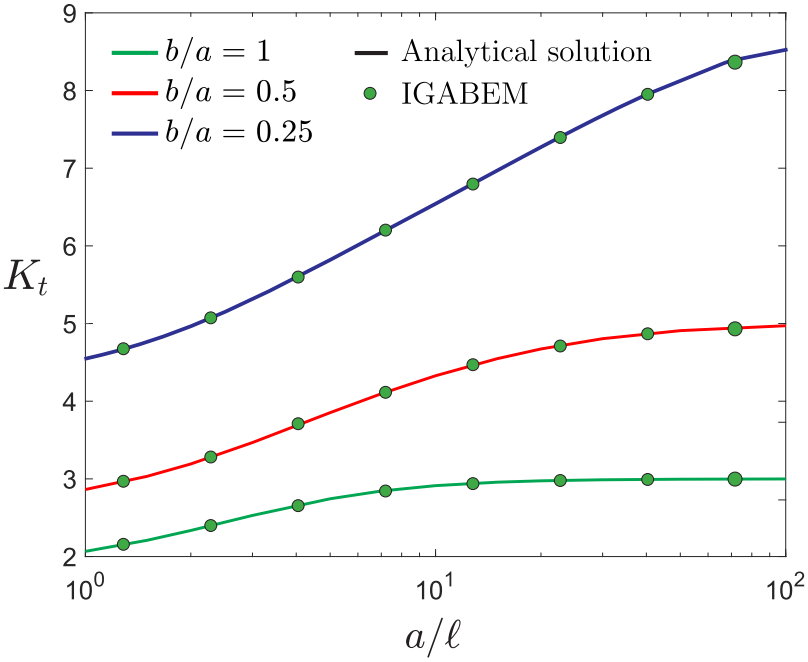

Fig. 5. Variation of stress concentration factor with a/ℓ for the elliptical opening.

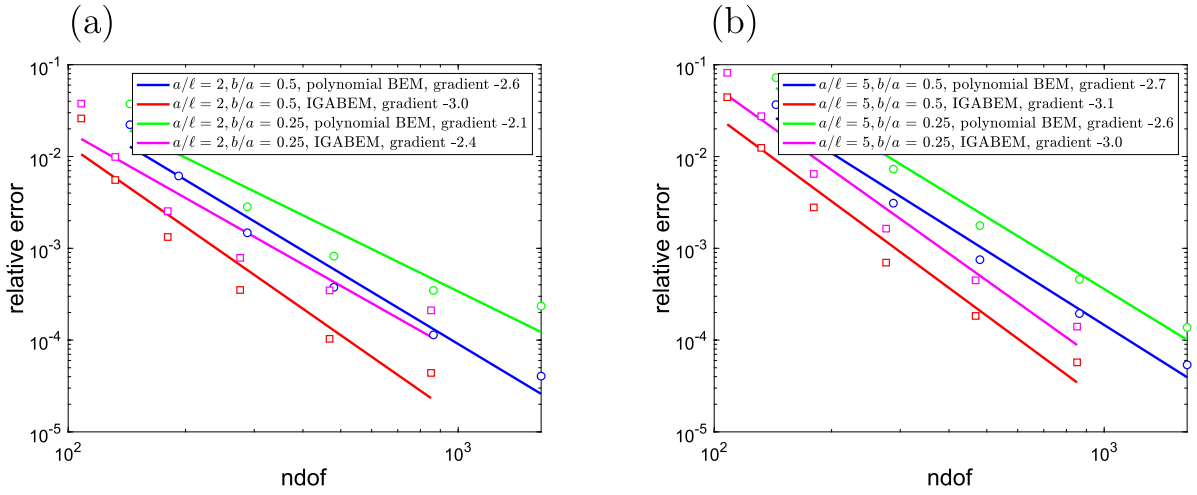

Fig. 6. Convergence for elliptical opening: (a) $a/\ell = 2$ and (b) $a/\ell = 5$.

We plot convergence for the cases $a/\ell = \{2, 5\}$ in Fig. 6. Once again, it is evident that the NURBS basis affords the IGABEM scheme advantageous convergence properties in comparison with the conventional piecewise polynomial basis.

In Table 4, we compare the ellipse stress concentration factors as produced by different BEM schemes. We list also our analytical solution, and reproduce the results of Lei et al. [33], who used a quarter-symmetric model comprising 68 elements. It is difficult to draw a reliable comparison with [33] because, although the number of elements is given, it is not clear how those authors performed numerical integration, nor how they implemented the symmetry. However, 68 continuous, quadratic elements would correspond to 408 degrees of freedom to model the quarter plate, and in the table we compare those results against the use of 480 (polynomial) and 468 (IGABEM) degrees of freedom to model the *complete* plate. The IGABEM results are in a very good agreement with the analytical solution illustrating that the IGABEM formulation is capable of delivering highly accurate solutions.

Table 4
Comparison of K_t results for elliptical opening from different schemes.

a/ℓ	b/a	Analytical solution	Lei et al. [33]	Polynomial 480 dof	IGABEM 468 dof
1	0.5	2.8630	2.8203	2.8627	2.8630
	0.25	4.5495	4.4093	4.5487	4.5494
2	0.5	3.1920	3.1660	3.1909	3.1918
	0.25	4.9683	4.8225	4.9652	4.9676
20	0.5	4.6725	4.7019	4.6691	4.6718
	0.25	7.2719	6.6824	7.2453	7.2660

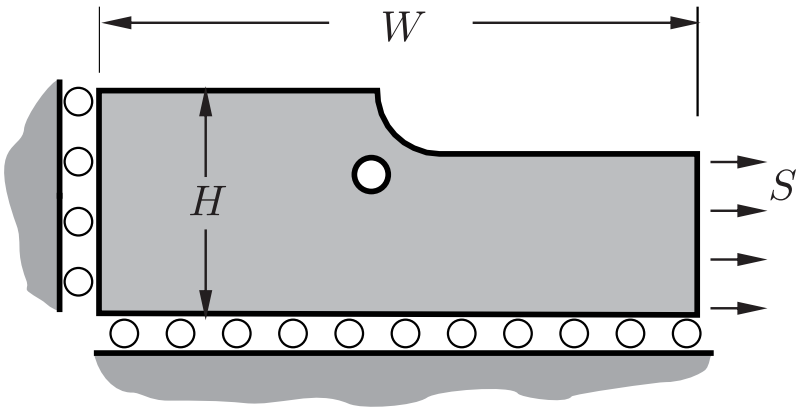

Fig. 7. Strip containing a hole near a shoulder fillet.

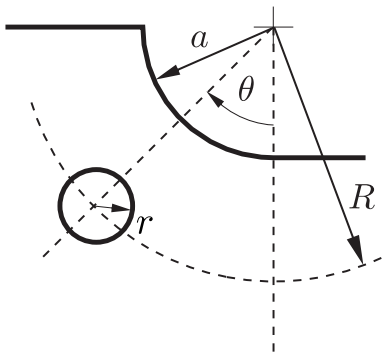

Fig. 8. Geometric detail and parametric definitions.

7.3. Hole near shoulder fillet

We close by considering an example demonstrating the flexibility of the numerical method presented in this article, a flexibility inherited from its basis in the boundary element method. No reference solutions are available, but we present the results in the spirit of Peterson [59] and later Pilkey [60], which are popular sources for design engineers requiring stress concentration factors for a wide variety of situations. We present results for a plane strain strip containing a hole near a shoulder fillet.

The geometry is presented in Fig. 7, and consists of a strip of length W and height H, acted on by a horizontal stress S on its right hand edge. Roller boundary conditions are applied to the left and bottom edges with null couple stresses at all boundaries. Fig. 8 presents a detailed view of the geometry of the shoulder fillet, of radius a,

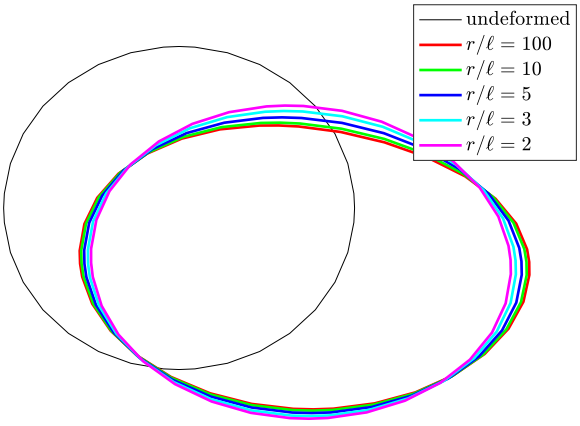

Fig. 9. Deformed shape of the hole, with different characteristic lengths.

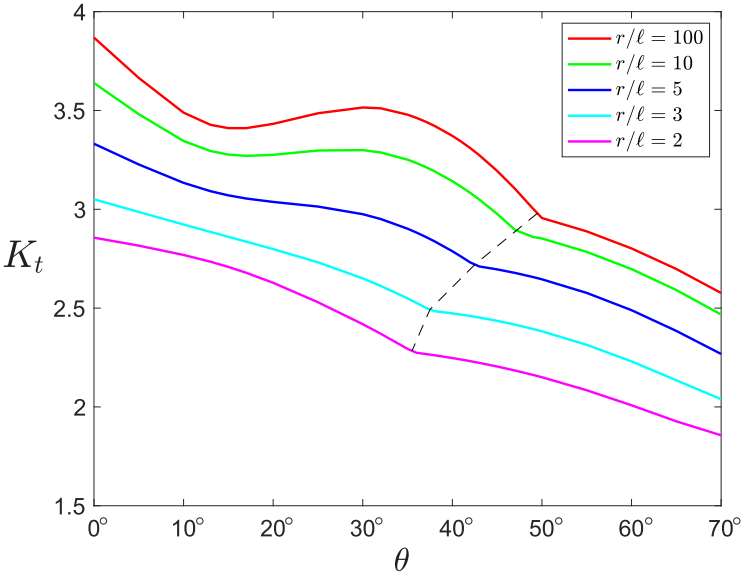

Fig. 10. Stress concentration factors for hole near shoulder fillet.

and circular hole of radius r. The centre of the hole is located in the polar coordinate system (R, θ) as shown in the Figure.

For our study we consider the geometry given by $R/a = 2, r/a = 0.5$ and Poisson's ratio $\nu = 0.3$. The outer boundary is meshed using 116 elements of approximately uniform size, with a further 32 elements used to model the circular hole. No convergence study is performed but the mesh density is informed by the convergence studies contained in the preceding sections. The IGABEM formulation is used with a NURBS basis of degree $p = 2$, so that the model consists of a total of 474 degrees of freedom.

Fig. 9 shows the deformed shape of the hole, for the case $\theta = 45°$, when analysed using different characteristic lengths expressed nondimensionally as $r/\ell = \{2, 3, 5, 10, 100\}$. This shows the shape of the deformed hole to become more elongated for small characteristic lengths, i.e. as we approach the classical elasticity solution. Finally, Fig. 10 shows the variation of the stress concentration factor, defined as in (75), with angle θ and the dimensionless ratio r/ℓ. It is shown the variation of ℓ has a marked effect on the stress concentration factor, with the introduction of couple stresses having a beneficial effect in reducing the peak stress experienced as ℓ increases. Such a behaviour confirms the well documented stiffening size effects that are observed in cases where the material microstructure becomes comparable to the geometrical characteristics of the body. Generally K_t is seen also to reduce as θ

increases, owing to the increased shadowing of the hole by the shoulder fillet, though a peak at $\theta \approx 30^\circ$ for $r/\ell > 5$ shows that the interaction between the stress concentrations at the hole and fillet becomes complicated.

The curves for all characteristic lengths exhibit a 'knee' somewhere in the range $30 < \theta < 50^\circ$. This is the result of the location of the maximum stress changing with different locations of the hole as measured by angle θ. For the portions of the curves to the left of the knee, i.e. for small θ, the peak stress lies close to the top of the hole between 12 o'clock and 1 o'clock on the clock face. Conversely, for larger θ the peak stress lies close to the bottom of the hole, between 6 o'clock and 7 o'clock. A dashed line is included on the graph to demarcate these two regions, and it is interesting to note that the position (in θ) of the knee is a function of characteristic length.

This final study shows that engineers working with foams, and other cellular materials that exhibit a characteristic length that cannot be considered small in comparison with feature sizes, would benefit from extensions to [59,60] for use with these classes of material.

8. Conclusions

In the present work, we have developed an isogeometric boundary element method (IGABEM) for plane strain problems in couple stress elasticity. The IGABEM is very well suited for boundary value problems treated in the frame of generalized continuum theories due to the higher order continuity requirements imposed on the field quantities. Using a Fourier transform analysis, the fundamental solutions of the theory are obtained in closed form. Accordingly, employing the reciprocal theorem, two boundary integral equations are derived for the displacement and the rotation. An analytical solution is also derived for the elliptical hole plane strain problem in couple stress elasticity. The IGABEM formulation is validated against the derived analytical solutions but also with the results obtained by a conventional polynomial BEM also developed in the present study. It is shown that the IGABEM scheme exhibits superior convergence properties in comparison with standard BEM formulations. The results for the stress concentration problems examined in the present work exhibit considerable deviations from the predictions of classical elasticity. These deviations are more pronounced when the size of the geometrical defects becomes comparable to the characteristic material length of the couple stress theory. In such cases, stiffening size effects are observed which are in accordance with experimental observations in microstructured materials.

Finally, we note that the present formulation allows for the analysis of problems with more complex geometries and can be readily extended to deal with boundary value problems that exhibit strong discontinuities such as cracks and contact problems in Cosserat materials.

Declaration of competing interest

The authors declare that they have no known competing financial interests or personal relationships that could have appeared to influence the work reported in this paper.

Data availability

Data will be made available on request.

Acknowledgment

This research did not receive any specific grant from funding agencies in the public, commercial, or not-for-profit sectors.

Appendix A. Derivation of fundamental solutions

The static 2D Green's functions for an isotropic couple stress medium under plane strain conditions are derived in this Appendix. The analysis is based on the double Fourier transform. The direct (FT) and inverse (FT^{-1}) double Fourier transforms are defined, respectively, as

$$\hat{f}(\mathbf{k}) = \mathrm{FT}\{f(\mathbf{r})\} = \int_{\mathcal{R}^2} f(\mathbf{x}) e^{\mathrm{i}\ \mathbf{r}\cdot\mathbf{k}}\, d\mathbf{x}, \tag{A.1}$$

$$f(\mathbf{x}) = \mathrm{FT}^{-1}\{\hat{f}(\mathbf{k})\} = \frac{1}{(2\pi)^2} \int_{\mathcal{R}^2} \hat{f}(\mathbf{k}) e^{-\mathrm{i}\ \mathbf{r}\cdot\mathbf{k}}\, d\mathbf{k}. \tag{A.2}$$

where $r_q = x_q - \xi_q$ with $r = (r_q r_q)^{1/2}$, k_q is the Fourier vector with $k = (k_q k_q)^{1/2}$, and i is the imaginary unit.

Applying the Fourier transform to the equilibrium Eq. (9) and using its well-known properties we obtain

$$\mu \left[e_{qp} e_{mn} \ell^2 k^2 k_p k_m \hat{u}_n - k^2 \hat{u}_q - \frac{1}{1-2\nu} k_q k_p \hat{u}_p \right] + \hat{X}_q - \frac{\mathrm{i}}{2} e_{qp} k_p \hat{Y}_3 = 0. \tag{A.3}$$

To compute the transformed displacement $\hat{u}_k$, we exploit the antisymmetric properties of the permutation tensor e_{qp} and multiply (A.3) by k_q, which leads to

$$k_q \hat{u}_q = \frac{(1-2\nu)\hat{X}_q k_q}{2\mu(1-\nu)k^2}. \tag{A.4}$$

Next, the two dimensional $e-\delta$ identity: $e_{qp}e_{mn} = \delta_{qm}\delta_{pn} - \delta_{qn}\delta_{pm}$ is used in (A.3) in conjunction with (A.4), which after some lengthy manipulations yields the following solution for the transformed displacement field

$$\mu \hat{u}_q = \frac{1}{k^2(1+\ell^2 k^2)} \left[\frac{(1-2\nu)k_q k_p}{2(1-\nu)k^2} (\ell^2 k^2 - \frac{1}{1-2\nu}) + \delta_{qp} \right] \hat{X}_p - \frac{\mathrm{i}\, e_{qp} k_p}{2k^2(1+\ell^2 k^2)} \hat{Y}_3. \tag{A.5}$$

A.1. Concentrated force

The 2D infinite body Green's function will be now obtained for a concentrated unit force ($\mathcal{F}$): $X_q = \delta_{qk}\delta(\boldsymbol{r})\boldsymbol{e}_k$, applied at point $\boldsymbol{\xi}$ in the kth-direction, where $\delta(\boldsymbol{r}) = \delta(r_1)\delta(r_2)$ is the Dirac delta distribution. The displacement is then defined as $u_q = U^{(\mathcal{F})}_{qk}\boldsymbol{e}_k$ denoting the displacement at point $\boldsymbol{x}$ in the qth-direction due to a unit force at point $\boldsymbol{\xi}$ in the kth-direction. Further, we have that: $\hat{X}_p = \delta_{pk}\boldsymbol{e}_k$ and $\hat{Y} = 0$. In view of the above, the transformed displacement $\hat{u}_q = \hat{U}^{(\mathcal{F})}_{qk}\boldsymbol{e}_k$, in (A.5) can be written in following form

$$\mu \hat{U}^{(\mathcal{F})}_{qk} = \frac{\delta_{qk}}{k^2} - \frac{k_q k_k}{2(1-\nu)k^4} + \frac{\ell^2 k_q k_k}{k^2} - \frac{\ell^2(\delta_{qk} + \ell^2 k_q k_k)}{1+\ell^2 k^2}. \tag{A.6}$$

The inversion of the transformed solution is accomplished by utilizing well-known results regarding double Fourier transforms (see e.g. [61,62]). In particular, we have that

$$\begin{aligned} \mathfrak{I}_1 = \mathrm{FT}^{-1}\{k^{-2}\} = -\frac{1}{2\pi}(\gamma + \ln r), \qquad \mathfrak{I}_2 = \mathrm{FT}^{-1}\{k^{-4}\} = \frac{r^2}{8\pi}(\gamma + \ln r), \\ \mathfrak{I}_3 = \mathrm{FT}^{-1}\{(1+\ell^2 k^2)^{-1}\} = \frac{1}{2\pi\ell^2} K_0. \end{aligned} \tag{A.7}$$

where γ is the Euler constant and $K_n \equiv K_n[r/\ell]$ is the modified second kind Bessel function of the nth-order. Note that the first and second integrals in (A.7) are to be interpreted in the finite-part sense. Accordingly, it may be readily inferred that

$$\begin{aligned} \mathrm{FT}^{-1}\{k_q k_k k^{-2}\} &= -[\mathfrak{I}_1]_{,qk} = \frac{1}{2\pi r^2}(\delta_{qk} - 2r_{,q}r_{,k}), \\ \mathrm{FT}^{-1}\{k_q k_k k^{-4}\} &= -[\mathfrak{I}_2]_{,qk} = -\frac{1}{8\pi}\Big((1+2\gamma)\delta_{qk} + 2r_{,q}r_{,k} + 2\delta_{qk}\ln r\Big), \\ \mathrm{FT}^{-1}\{k_q k_k (1+\ell^2 k^2)^{-1}\} &= -[\mathfrak{I}_3]_{,qk} = \frac{1}{4\pi\ell^4}\Big((K_2 - K_0)\delta_{qk} - 2r_{,q}r_{,k}K_2\Big). \end{aligned} \tag{A.8}$$

where the differentiation in the above relations is taken w.r.t. the variable $\boldsymbol{x}$. Gathering the above results and neglecting rigid body motions, we derive Eq. (10) which is the 2D infinite body Green's function for the displacement field due to a concentrated force. Accordingly, the displacement gradient assumes the following form

$$\begin{aligned} U^{(\mathcal{F})}_{qk,m} = \frac{1}{8\mu\pi(1-\nu)r}&\Big(\delta_{qm}r_{,k} + \delta_{km}r_{,q} - (3-4\nu)\delta_{qk}r_{,m} - 2r_{,q}r_{,k}r_{,m}\Big) \\ &- \frac{1}{2\pi\mu r}\left(\frac{2\ell^2}{r^2} - K_2\right)\Big(\delta_{qm}r_{,k} + \delta_{km}r_{,q} + \delta_{qk}r_{,m} - 4r_{,q}r_{,k}r_{,m}\Big) \\ &+ \frac{1}{2\pi\mu\ell}\Big(\delta_{qk} - r_{,q}r_{,k}\Big)r_{,m}K_1. \end{aligned} \tag{A.9}$$

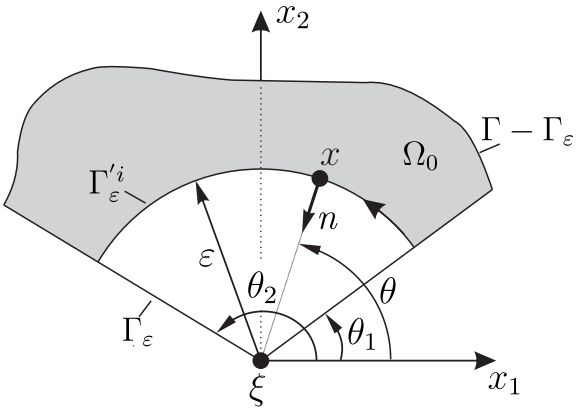

Fig. B.1. Definition of the boundary Γ'^i_ε when the corner point $\boldsymbol{\xi}$ belongs to the original boundary Γ.

A.2. Concentrated couple

The 2D infinite body Green's function will be now obtained for a concentrated out-of-plane unit couple ($\mathcal{M}$): $Y \equiv Y_3 = \delta(\boldsymbol{r})$ at the x_3-direction. The displacement vector is defined as $u_q = U_q^{(\mathcal{M})}(\mathbf{x};\boldsymbol{\xi})$ denoting the displacement at point $\boldsymbol{x}$ in the kth-direction due to the unit couple at point $\boldsymbol{\xi}$. Further, we have that: $\hat{X}_q = 0$ and $\hat{Y} = 1$. In view of the above, the transformed displacement $\hat{U}_q^{(\mathcal{M})}$, in (A.5) assumes the following form

$$\mu \hat{U}_q^{(\mathcal{M})} = \frac{\mathrm{i}\,\ell^2 e_{qp}}{2}\left(-\frac{k_p}{\ell^2 k^2} + \frac{k_p}{1+\ell^2 k^2}\right). \tag{A.10}$$

The inversion of the transformed solution (A.10) is based on the results in (A.7). In particular, we have that

$$\mathrm{FT}^{-1}\{\mathrm{i}\,k_p k^{-2}\} = -[\mathfrak{I}_1]_{,p} = \frac{r_{,p}}{2\pi r}, \quad \mathrm{FT}^{-1}\{\mathrm{i}\,k_p(1+\ell^2 k^2)^{-1}\} = -[\mathfrak{I}_3]_{,p} = \frac{r_{,p}}{2\pi \ell^3} K_1. \tag{A.11}$$

Gathering the above results, we derive Eq. (15) which is the 2D infinite body Green's function for the displacement field due to a concentrated couple.

Finally, we note that the Green's function for a concentrated couple could have been alternatively derived in the couple stress theory by setting $Y = 0$ and assuming a body force of the type $X_q = (1/2)e_{qp}\partial_p \delta(\boldsymbol{r})$. This is because the rotation and the displacements are not independent but related through the first of Eqs (3).

Appendix B. Evaluation of the free terms

The coefficient matrix c_{pq} of the free term is evaluated in the context of couple stress elasticity for a non-smooth boundary. The coefficient matrix depends on the local geometry at the neighbourhood of point $\boldsymbol{\xi}$ to which the integral equation refers. Here, for simplicity it is assumed that two flat surfaces define the neighbourhood of the corner point $\boldsymbol{\xi}$ as shown in Fig. B.1. Further, we isolate point $\boldsymbol{\xi}$ as shown in Fig. B.1, so that the arc Γ'^i_ε is the part of the circle with radius ε centred at $\boldsymbol{\xi}$ which is inside the domain Ω. Also, we define the closed boundary $\Gamma_0 = \Gamma - \Gamma_\varepsilon + \Gamma'^i_\varepsilon$ which encloses the domain Ω_0 (Fig. B.1). The concept of a rigid body translation is employed to determine the coefficient matrix c_{pq}. For a constant displacement field $u^\star_q$, we obtain

$$u_q = u^\star_q, \quad \omega = 0, \quad t_q = 0, \quad \mathfrak{s} = 0. \tag{B.1}$$

The coefficient matrix in Eq. (25) is then given as

$$c_{qk} = -\!\!\!\!\!\!\int_\Gamma T^{(\mathcal{F})}_{qk}\, d\Gamma_x \tag{B.2}$$

By noting that $\int_{\Gamma_0} = \int_{\Gamma-\Gamma_\varepsilon} + \int_{\Gamma_\varepsilon'^i}$ and taking $\varepsilon \to 0$, we may write

$$\lim_{\varepsilon\to 0}\int_{\Gamma_0} T_{qk}^{(\mathcal{F})}\, d\Gamma_x = 0 \Rightarrow \lim_{\varepsilon\to 0}\int_{\Gamma-\Gamma_\varepsilon} T_{qk}^{(\mathcal{F})}\, d\Gamma_x + \lim_{\varepsilon\to 0}\int_{\Gamma_\varepsilon'^i} T_{qk}^{(\mathcal{F})}\, d\Gamma_x = \oint_{\Gamma} T_{qk}^{(\mathcal{F})}\, d\Gamma_x + \lim_{\varepsilon\to 0}\int_{\Gamma_\varepsilon'^i} T_{qk}^{(\mathcal{F})}\, d\Gamma_x = 0, \tag{B.3}$$

where we have used the fact that the integral over Γ_0 vanishes since the point $\boldsymbol{\xi} \notin \bar{\Omega}_0$ (force traction equilibrium). Combining (B.2) and (B.3), we have that

$$c_{qk} = \lim_{\varepsilon\to 0}\int_{\Gamma_\varepsilon'^i} T_{qk}^{(\mathcal{F})}\, d\Gamma_x = \lim_{\varepsilon\to 0}\int_{\Gamma_\varepsilon'^i} \Sigma_{pqk}^{(\mathcal{F})} n_p\, d\Gamma_x = \lim_{\varepsilon\to 0}\int_{\theta_1}^{\theta_2} \Sigma_{pqk}^{(\mathcal{F})} n_p\, \varepsilon d\theta. \tag{B.4}$$

The integrals in (B.4) can be evaluated analytically using (13) and the following geometric relations according to Fig. B.1

$$\begin{aligned} &\boldsymbol{r} = (\varepsilon\cos\theta, \varepsilon\sin\theta), \quad \boldsymbol{n} = (-\cos\theta, -\sin\theta),\\ &r = |\boldsymbol{r}| = \varepsilon, \quad \partial r/\partial n = -1, \quad r_{,i} = -n_i, \quad \text{on } \Gamma_\varepsilon'^i. \end{aligned} \tag{B.5}$$

Taking the limit as $\varepsilon \to 0$, we derive

$$\begin{aligned} c_{11} &= \frac{\beta}{2\pi} - \frac{(1-2\nu)\sin\beta\cos 2\gamma}{4\pi(1-\nu)},\\ c_{12} = c_{21} &= -\frac{(1-2\nu)\sin\beta\sin 2\gamma}{4\pi(1-\nu)},\\ c_{22} &= \frac{\beta}{2\pi} + \frac{(1-2\nu)\sin\beta\cos 2\gamma}{4\pi(1-\nu)}, \end{aligned} \tag{B.6}$$

where $\beta = \theta_2 - \theta_1$ and $\gamma = (\theta_2 + \theta_1)/2$. Note that the expressions (B.6) do not involve the characteristic length ℓ and also do not coincide with their classical counterparts [63]. The difference in the expressions of the components of the free term c_{pq} in the classical theory and the couple stress theory is attributed to strong boundary layer effects that emerge in the case of a non-smooth boundary. In particular, it can be readily verified that $\lim_{\substack{\ell\to 0\\ \varepsilon\to 0}} \int_{\Gamma_\varepsilon'^i} T_{qk}^{(\mathcal{F})}\, d\Gamma_x \neq \lim_{\substack{\varepsilon\to 0\\ \ell\to 0}} \int_{\Gamma_\varepsilon'^i} T_{qk}^{(\mathcal{F})}\, d\Gamma_x$. Such boundary layer effects have been also observed by Bogy and Sternberg [64] in corner problems in couple stress elasticity (see also [38]). Nonetheless, for a smooth boundary ($\beta = \pi$), we obtain in both theories that: $c_{pq} = 1/2\delta_{pq}$.

Following an analogous procedure, we can determine the free term c_o in Eq. (26). For a constant displacement field $u_q = u_q^\star$, we immediately infer that: $\int_\Gamma T_q^{(\mathcal{M})} d\Gamma_x = 0$. Further, for a constant rotation field $\omega = \omega^\star$, the corresponding displacement field becomes $u_q = u_q^\star + e_{mq} r_m \omega^\star$ with $r_m = x_m - \xi_m$, and $t_q = 0$, $\mathfrak{s} = 0$. In this case, (26) is written as

$$c_o = -\int_\Gamma e_{mq} r_m T_q^{(\mathcal{M})} d\Gamma_x - \oint_\Gamma S^{(\mathcal{M})} d\Gamma_x. \tag{B.7}$$

On the other hand, indenting the contour Γ as shown in Fig. B.1, we may write

$$\begin{aligned} \lim_{\varepsilon\to 0}\int_{\Gamma_0} (e_{mq} r_m T_q^{(\mathcal{M})} + S^{(\mathcal{M})})\, d\Gamma_x &= \lim_{\varepsilon\to 0}\int_{\Gamma-\Gamma_\varepsilon} e_{mq} r_m T_q^{(\mathcal{M})}\, d\Gamma_x + \int_{\Gamma-\Gamma_\varepsilon} S^{(\mathcal{M})}\, d\Gamma_x +\\ &+ \lim_{\varepsilon\to 0}\int_{\Gamma_\varepsilon'^i} e_{mq} r_m T_q^{(\mathcal{M})}\, d\Gamma_x + \lim_{\varepsilon\to 0}\int_{\Gamma_\varepsilon'^i} S^{(\mathcal{M})}\, d\Gamma_x =\\ \int_\Gamma e_{mq} r_m T_q^{(\mathcal{M})} d\Gamma_x + \oint_\Gamma S^{(\mathcal{M})}\, d\Gamma_x &+ \lim_{\varepsilon\to 0}\int_{\Gamma_\varepsilon'^i} S^{(\mathcal{M})}\, d\Gamma_x = 0. \end{aligned} \tag{B.8}$$

The integral over Γ_0 in (B.8) represents the conservation of angular momentum in the body and vanishes since the point $\boldsymbol{\xi} \notin \bar{\Omega}_0$. Note also that based on the asymptotic properties of the traction $T_q^{(\mathcal{M})}$ (see Table 2) the fourth integral in (B.8) vanishes too as $\varepsilon \to 0$. Hence, combining Eqs. (B.7) and (B.8) and taking into account (19), we finally derive

$$c_o = \lim_{\varepsilon\to 0}\int_{\Gamma_\varepsilon'^i} S^{(\mathcal{M})}\, d\Gamma_x = \lim_{\varepsilon\to 0}\int_{\Gamma_\varepsilon'^i} M_p^{(\mathcal{M})} n_p\, d\Gamma_x = \lim_{\varepsilon\to 0}\int_{\theta_1}^{\theta_2} M_p^{(\mathcal{M})} n_p\, \varepsilon d\theta = \frac{\beta}{2\pi}. \tag{B.9}$$

Note that for a smooth boundary we have that $c_o = 1/2$.

Appendix C. Analytical solution for an elliptical hole

For the determination of the M coefficients $\{w_m, h_m, g_m\}$, we employ the modified Schmidt orthogonalization process as described in [50,52]. Note that summation convention is not used in this section. As a first step, we construct orthogonal functions $\mathcal{F}_m^{(\mu)}$ from the functions $\mathcal{G}_m^{(\mu)}$ in the following way

$$\mathcal{F}_m^{(\mu)}(\eta) = \sum_{i=1}^{m} \frac{\text{cof}(\pi_{im})}{\text{cof}(\pi_{mm})} \mathcal{G}_i^{(\mu)}(\eta) \quad \text{with} \quad \pi_{ij} = \int_0^\pi \mathcal{G}_i^{(\mu)}(\eta)\, \mathcal{G}_j^{(\mu)}(\eta)\, d\eta, \tag{C.1}$$

and

$$\int_0^\pi \mathcal{F}_m^{(\mu)}(\eta)\, \mathcal{F}_n^{(\mu)}(\eta)\, d\eta = \mathfrak{J}_m \delta_{mn} \quad \text{and} \quad \mathfrak{J}_m = \int_0^\pi \left[\mathcal{F}_m^{(\mu)}(\eta)\right]^2 d\eta. \tag{C.2}$$

Note that $\text{cof}(\pi_{im})$ is the cofactor of the element $[im]^{th}$ of the symmetric $m \times m$ matrix π_{ij}. From (70), we may write

$$\sum_{m=1}^{M} g_m\, \mathcal{G}_m^{(\mu)}(\eta) = \sum_{m=1}^{M} \varepsilon_m\, \mathcal{F}_n^{(\mu)}(\eta) = -\sum_{m=1}^{M} h_m \mathcal{H}_m^{(\mu)}(\eta), \tag{C.3}$$

where

$$\varepsilon_m = -\frac{1}{\mathfrak{J}_m} \sum_{i=1}^{M} \Big[h_i \int_0^\pi \mathcal{H}_i^{(\mu)}(\eta) \mathcal{F}_m^{(\mu)}(\eta) d\eta \Big],$$

and thus we obtain

$$g_m = \sum_{i=1}^{M} \rho_{mi} h_i, \quad \text{with} \quad \rho_{mi} = -\sum_{j=m}^{M} \frac{\text{cof}(\pi_{mj})}{\text{cof}(\pi_{jj})} \frac{1}{\mathfrak{J}_j} \int_0^\pi \mathcal{H}_i^{(\mu)}(\eta) F_j^{(\mu)}(\eta) d\eta. \tag{C.4}$$

Substituting (C.4), into Eqs (68) and (69), we obtain

$$\sum_{m=1}^{M} \Big[w_m\, \mathcal{W}_m^{(\sigma)}(\eta) + h_m\, \mathcal{H}_m^{*(\sigma)}(\eta) \Big] = -s(\eta), \tag{C.5}$$

$$\sum_{m=1}^{M} \Big[w_m\, \mathcal{W}_m^{(\tau)}(\eta) + h_m\, \mathcal{H}_m^{*(\tau)}(\eta) \Big] = -\tau(\eta), \tag{C.6}$$

where

$$\mathcal{H}_m^{*(\sigma)}(\eta) = \mathcal{H}_m^{(\sigma)}(\eta) + \sum_{i=1}^{M} \rho_{im} \mathcal{G}_i^{(\sigma)}(\eta) \quad \text{and} \quad \mathcal{H}_m^{*(\tau)}(\eta) = \mathcal{H}_m^{(\tau)}(\eta) + \sum_{i=1}^{M} \rho_{im} \mathcal{G}_i^{(\tau)}(\eta).$$

The same procedure is employed in order to construct the orthogonal functions $F_m^{(\tau)}(\eta)$ from $\mathcal{H}^{*(\tau)}$,

$$\mathcal{F}_m^{(\tau)}(\eta) = \sum_{i=1}^{m} \frac{\text{cof}(\pi_{im}^*)}{\text{cof}(\pi_{mm}^*)} \mathcal{H}_i^{*(\tau)}(\eta) \quad \text{with} \quad \pi_{ij}^* = \int_0^\pi \mathcal{H}_i^{*(\tau)}(\eta) \mathcal{H}_j^{*(\tau)}(\eta)\, d\eta, \tag{C.7}$$

where $\text{cof}(\pi_{im}^*)$ is the cofactor of the element $[im]^{th}$ of the symmetric $m \times m$ matrix π_{ij}^*. In this way, we obtain the coefficients h_m as

$$h_m = \sum_{i=1}^{M} \rho_{mi}^* w_i + \varepsilon_m^*, \quad \text{with} \quad \rho_{mi}^* = -\sum_{j=m}^{M} \frac{\text{cof}(\pi_{mj}^*)}{\text{cof}(\pi_{jj}^*)} \frac{1}{\mathfrak{J}_j^*} \int_0^\pi \mathcal{H}_i^{*(\tau)}(\eta) F_j^{(\tau)}(\eta) d\eta, \tag{C.8}$$

and

$$\varepsilon_m^* = -\sum_{j=m}^{M} \frac{\text{cof}(\pi_{mj}^*)}{\text{cof}(\pi_{jj}^*)} \frac{1}{\mathfrak{J}_j^*} \int_0^\pi \tau(\eta) F_j^{(\tau)}(\eta) d\eta, \qquad \mathfrak{J}_m^* = \int_0^\pi \left[\mathcal{F}_m^{(\tau)}(\eta)\right]^2 d\eta. \tag{C.9}$$

Substituting (C.8) into Eqs (C.5), we obtain

$$\sum_{m=1}^{M} w_m \mathcal{W}_m^{*(\sigma)}(\eta) = -s(\eta) - \sum_{i=1}^{M} \varepsilon_i^* \mathcal{H}_i^{*(\sigma)}(\eta), \tag{C.10}$$

where

$$\mathcal{W}_m^{*(\sigma)}(\eta) = \mathcal{W}_m^{(\sigma)}(\eta) + \sum_{i=1}^{M} \rho_{im}^* \mathcal{H}_i^{*(\sigma)}(\eta). \tag{C.11}$$

Finally, we construct the orthogonal functions $F_m^{(\sigma)}(\eta)$ from $\mathcal{W}^{*(\sigma)}$ as

$$\mathcal{F}_m^{(\sigma)}(\eta) = \sum_{i=1}^{m} \frac{\operatorname{cof}(\pi_{im}^{**})}{\operatorname{cof}(\pi_{mm}^{**})} \mathcal{W}_i^{*(\sigma)}(\eta) \quad \text{with} \quad \pi_{ij}^{**} = \int_0^{\pi} \mathcal{W}_i^{*(\sigma)}(\eta) \mathcal{W}_j^{*(\sigma)}(\eta)\, d\eta. \tag{C.12}$$

In this way, we obtain after some lengthy manipulations the coefficients w_m as,[2]

$$w_m = -\sum_{j=m}^{M} \left\{ \frac{\operatorname{cof}(\pi_{mj}^{**})}{\operatorname{cof}(\pi_{jj}^{**})} \frac{1}{\mathfrak{J}_j^{**}} \int_0^{\pi} s(\eta) F_j^{(\sigma)}(\eta) d\eta + \sum_{i=1}^{M} \varepsilon_i^* \int_0^{\pi} F_j^{(\sigma)}(\eta) \mathcal{H}_i^{*(\sigma)}(\eta) d\eta \right\}, \tag{C.13}$$

with

$$\mathfrak{J}_m^{**} = \int_0^{\pi} \left[\mathcal{F}_m^{(\sigma)}(\eta) \right]^2 d\eta. \tag{C.14}$$

Once the coefficients w_m are known, h_m and g_m can be evaluated from (C.4) and (C.8), respectively. Note that all integrals are evaluated numerically using the standard Gauss–Legendre quadrature.

References

[1] E. Cosserat, F. Cosserat, Théorie Des Corps Déformables, Hermann, Paris, 1909.
[2] R.A. Toupin, Elastic materials with couple-stresses, Arch. Ration. Mech. Anal. 11 (1962) 385–414.
[3] R.D. Mindlin, H.F. Tiersten, Effects of couple-stresses in linear elasticity, Arch. Ration. Mech. Anal. 11 (1962) 415–448.
[4] D. Bigoni, W.J. Drugan, Analytical derivation of Cosserat moduli via homogenization of heterogeneous elastic materials, J. Appl. Mech. 74 (2007) 741–753.
[5] N. Auffray, R. Bouchet, Y. Brechet, Strain gradient elastic homogenization of bidimensional cellular media, Int. J. Solids Struct. 47 (13) (2010) 1698–1710.
[6] M. Bacca, D. Bigoni, F. Dal Corso, D. Veber, Mindlin second-gradient elastic properties from dilute two-phase Cauchy-elastic composites. Part I: Closed form expression for the effective higher-order constitutive tensor, Int. J. Solids Struct. 50 (24) (2013) 4010–4019.
[7] G. Rizzi, F. Dal Corso, D. Veber, D. Bigoni, Identification of second-gradient elastic materials from planar hexagonal lattices. Part I: Analytical derivation of equivalent constitutive tensors, Int. J. Solids Struct. 176 (2019) 1–18.
[8] E. Radi, On the effects of characteristic lengths in bending and torsion on mode III crack in couple stress elasticity, Int. J. Solids Struct. 45 (2008) 3033–3058.
[9] A. Piccolroaz, G. Mishuris, E. Radi, Mode III interfacial crack in the presence of couple-stress elastic materials, Eng. Fract. Mech. 80 (2012) 60–71.
[10] P.A. Gourgiotis, A. Piccolroaz, Steady-state propagation of a mode II crack in couple stress elasticity, Int. J. Fract. 188 (2) (2014) 119–145.
[11] P.A. Gourgiotis, Interaction of shear cracks in microstructured materials modeled by couple-stress elasticity, J. Mech. Mater. Struct. 13 (3) (2018) 401–419.
[12] P.A. Gourgiotis, Th. Zisis, A.E. Giannakopoulos, H.G. Georgiadis, The Hertz contact problem in couple-stress elasticity, Int. J. Solids Struct. 168 (2019) 228–237.
[13] Y. Wang, X. Zhang, H. Shen, J. Liu, B. Zhang, S. Xu, Three-dimensional contact analysis with couple stress elasticity, Int. J. Mech. Sci. 153 (2019) 369–379.
[14] Y. Wang, X. Zhang, H. Shen, J. Liu, B. Zhang, Couple stress-based 3D contact of elastic films, Int. J. Solids Struct. 191–192 (2020) 449–463.
[15] E. Radi, A loaded beam in full frictionless contact with a couple stress elastic half-plane: Effects of non-standard contact conditions, Int. J. Solids Struct. 232 (2021) 111175.
[16] P. Li, T.J. Liu, The two-dimensional adhesive contact problem in the theory of couple stress elasticity, J. Adhes. Sci. Technol. 34 (10) (2020) 1062–1082.

[2] Note that in Itou [50] the second term inside the braces of (C.13) was inadvertently omitted.

[17] E. Radi, A. Nobili, M.A. Guler, Indentation of a free beam resting on an elastic substrate with an internal lengthscale, Eur. J. Mech. A Solids (2022) 104804.
[18] P.A. Gourgiotis, D. Bigoni, Stress channelling in extreme couple-stress materials, Part I: Strong ellipticity, wave propagation, ellipticity, and discontinuity relations, J. Mech. Phys. Solids 88 (2016) 150–168.
[19] P.A. Gourgiotis, D. Bigoni, Stress channelling in extreme couple-stress materials, Part II: Localized folding vs faulting of a continuum in single and cross geometries, J. Mech. Phys. Solids 88 (2016) 169–185.
[20] T.-M. Le, J. Lawongkerd, T.-Q. Bui, S. Limkatanyu, J. Rungamornrat, Elastic response of surface-loaded half plane with influence of surface and couple stresses, Appl. Math. Model. 91 (2021) 892–912.
[21] W. Wongviboonsin, T.-M. Le, J. Lawongkerd, P.A. Gourgiotis, J. Rungamornrat, Microstructural effects on the response of a multi-layered elastic substrate, Int. J. Solids Struct. 241 (2022) 111394.
[22] P.A. Gourgiotis, D. Bigoni, The dynamics of folding instability in a constrained Cosserat medium, Philos. Trans. R. Soc. Lond. A Math. Phys. Eng. Sci. 375 (2093) (2017) 20160159.
[23] A. Nobili, V. Volpini, C. Signorini, Antiplane Stoneley waves propagating at the interface between two couple stress elastic materials, Arch. Comp. Engng. 232 (3) (2021) 1207–1225.
[24] F.-Y. Huang, K.Z. Liang, Boundary element method for micropolar thermoelasticity, Eng. Anal. Bound. Elem. 17 (1) (1996) 19–26.
[25] K.-Z. Liang, F.-Y. Huang, Boundary element method for micropolar elasticity, Internat. J. Engrg. Sci. 34 (1996) 509–521.
[26] E. Shmoylova, S. Potapenko, L. Rothenburg, Boundary element analysis of stress distribution around a crack in plane micropolar elasticity, Internat. J. Engrg. Sci. 45 (2–8) (2007) 199–209.
[27] E. Atroshchenko, S.P.A. Bordas, Fundamental solutions and dual boundary element methods for fracture in plane Cosserat elasticity, Proc. R. Soc. Lond. Ser. A Math. Phys. Eng. Sci. 471 (2179) (2015) 20150216.
[28] E. Atroshchenko, J.S. Hale, J.A. Videla, S. Potapenko, S.P.A. Bordas, Micro-structured materials: Inhomogeneities and imperfect interfaces in plane micropolar elasticity, a boundary element approach, Eng. Anal. Bound. Elem. 83 (2017) 195–203.
[29] D. Polyzos, K.G. Tsepoura, S.V. Tsinopoulos, D.E. Beskos, A boundary element method for solving 2-D and 3-D static gradient elastic problems: Part I: Integral formulation, Comput. Methods Appl. Mech. Engrg. 192 (26–27) (2003) 2845–2873.
[30] G.F. Karlis, S.V. Tsinopoulos, D. Polyzos, D.E. Beskos, Boundary element analysis of mode I and mixed mode (I and II) crack problems of 2-D gradient elasticity, Comput. Methods Appl. Mech. Engrg. 196 (49–52) (2007) 5092–5103.
[31] G.F. Karlis, A. Charalambopoulos, D. Polyzos, An advanced boundary element method for solving 2D and 3D static problems in Mindlin's strain-gradient theory of elasticity, Internat. J. Numer. Methods Engrg. 83 (11) (2010) 1407–1427.
[32] A.R. Hadjesfandiari, G.F. Dargush, Boundary element formulation for plane problems in couple stress elasticity, Internat. J. Numer. Methods Engrg. 89 (5) (2012) 618–636.
[33] J. Lei, P. Ding, C. Zhang, Boundary element analysis of static plane problems in size-dependent consistent couple stress elasticity, Eng. Anal. Bound. Elem. 132 (2021) 399–415.
[34] J. Lei, X. Wei, P. Ding, C. Zhang, General displacement and traction BEM for plane couple-stress problems, Eng. Anal. Bound. Elem. 140 (2022) 59–69.
[35] A.R. Hadjesfandiari, G.F. Dargush, Couple stress theory for solids, Int. J. Solids Struct. 48 (18) (2011) 2496–2510.
[36] P. Neff, I. Münch, I.D. Ghiba, A. Madeo, On some fundamental misunderstandings in the indeterminate couple stress model. A comment on recent papers of AR Hadjesfandiari and GF Dargush, Int. J. Solids Struct. 81 (2016) 233–243.
[37] W.T. Koiter, Couple stresses in the theory of elasticity, I and II, Proc. K. Ned. Akad. Wet. (B) 67 (1964) 17–44.
[38] R. Muki, E. Sternberg, The influence of couple-stresses on singular stress concentrations in elastic solids, ZAMP 16 (1965) 611–648.
[39] R.D. Mindlin, Micro-structure in linear elasticity, Arch. Ration. Mech. Anal. 16 (1964) 51–78.
[40] R.N. Simpson, S.P.A. Bordas, H. Lian, J. Trevelyan, An isogeometric boundary element method for elastostatic analysis: 2D implementation aspects, Comput. Struct. 118 (2013) 2–12.
[41] E. Sternberg, Couple-stresses and singular stress concentrations in elastic solids, in: Mechanics of Generalized Continua, Springer, 1968, pp. 95–108.
[42] Y. Weitsman, Two dimensional singular solutions in infinite regions with couple-stresses, Q. Appl. Math. 25 (1968) 485–489.
[43] L. Dragoş, Fundamental solutions in micropolar elasticity, Internat. J. Engrg. Sci. 22 (1984) 265–275.
[44] A. R Hadjesfandiari, G.F. Dargush, Fundamental solutions for isotropic size-dependent couple stress elasticity, Int. J. Solids Struct. 50 (9) (2013) 1253–1265.
[45] M.F. Beatty, A reciprocal theorem in the linearized theory of couple-stresses, Acta Mech. 3 (1967) 154–166.
[46] L.A. Piegl, W. Tiller, The NURBS Book, Springer, Berlin, 1997.
[47] R.N. Simpson, S.P.A. Bordas, J. Trevelyan, T. Rabczuk, A two-dimensional isogeometric boundary element method for elastostatic analysis, Comput. Methods Appl. Mech. Engrg. 209–212 (2012) 87–100.
[48] R. Johnson, Higher order B-spline collocation at the Greville abscissae, Appl. Numer. Math. 52 (2005) 63–75.
[49] Y.C. Hsu, F.D. Ju, W.J. Wang, A couple-stresses elastic solution of an infinite tension plate bounded by an elliptical hole, J. Math. Anal. Appl. 40 (3) (1972) 708–722.
[50] S. Itou, The effect of couple-stresses on the stress concentration around an elliptic hole, Acta Mech. 16 (3) (1973) 289–296.
[51] H. Haftbaradaran, H.M. Shodja, Elliptic inhomogeneities and inclusions in anti-plane couple stress elasticity with application to nano-composites, Int. J. Solids Struct. 46 (16) (2009) 2978–2987.
[52] W.F. Yau, Axisymmetric slipless indentation of an infinite, elastic cylinder, SIAM J. Appl. Math. 15 (1) (1967) 219–227.
[53] S. Itou, Indentations of an elastic Cosserat layer by moving punches, ZAMM Z. Angew. Math. Mech. 52 (2) (1972) 93–99.
[54] R.D. Mindlin, Influence of couple-stresses on stress concentrations, Exp. Mech. 3 (1963) 1–7.
[55] E.G. Coker, L.N.G. Filon, A Treatise on Photoelasticity, Cambridge University Press, London, 1931.
[56] N.W. McLachlan, Theory and Application of Mathieu Functions, Oxford University Press, 1947.

[57] P.M. Naghdi, The effect of elliptic holes on the bending of thick plates, ASME J. Appl. Mech. 22 (1) (1955) 89–94.
[58] C.E. Inglis, Stresses in plates due to the presence of cracks and sharp corners, Trans. Inst. Naval Archit. 55 (1913) 219–241.
[59] R.E. Peterson, Stress Cconcentration Design Factors, second ed., Wiley, New York, 1974.
[60] W.D. Pilkey, D.F. Pilkey, Peterson's Stress Concentration Factors, third ed., Wiley, 2007.
[61] I.S. Gradshteyn, I.M. Ryzhik, Table of Integrals, Series, and Products, Academic Press, 2014.
[62] W. Nowacki, On discrete dislocations in micropolar elasticity, Arch. Mech. Stos 26 (1974) 3–11.
[63] F. Paris, J. Cañas, Boundary Element Method: Fundamentals and Applications, Oxford University Press, USA, 1997.
[64] D.B. Bogy, E. Sternberg, The effect of couple-stresses on the corner singularity due to an asymmetric shear loading, Int. J. Solids Struct. 4 (2) (1968) 159–174.